Single cell trajectory modeling identifies a primitive trophoblast state defined by BCAM enrichment

Matthew Shannon[1,2], Jennet Baltayeva[1,2], Barbara Castellana[1,2], Jasmin Wächter[1,2], Samantha Yoon[1,3], Jenna Treissman[1,2], Hoa Le[1,3], Alexander G. Beristain[1,2]

[1] The British Columbia Children's Hospital Research Institute, Vancouver, Canada.
[2] Department of Obstetrics & Gynecology, The University of British Columbia, Vancouver, Canada.
[3] Department of Surgery, The University of British Columbia, Vancouver, Canada.

To whom correspondence should be addressed: Alexander G. Beristain, The British Columbia Children's Hospital Research Institute, The University of British Columbia, Vancouver, British Columbia, Canada. V5Z 4H4. Tel: (604) 875-3573; E-mail: aberista@mail.ubc.ca

Keywords: Placenta, trophoblast, single cell RNA-sequencing, extravillous trophoblast, villous cytotrophoblast, cell differentiation,

Summary Statement: A trophoblast progenitor niche enriched in BCAM shows complex cell trajectory dynamics and gene signaling pathways

Abbreviations

CTB: Cytotrophoblast
DCT: Distal column trophoblast
DGE: Differential gene expression
EVT: Extravillous trophoblast
FDR: False discovery rate
GO: Gene ontology
HLA-G: Human leukocyte antigen G
Hr: Hour
RT: Room Temperature
IF: Immunofluorescence
PCT: Proximal column trophoblast
scRNA-seq: single cell RNA sequencing
SCT: Syncytiotrophoblast
UMAP: Uniform manifold approximation and projection
vCTB: Villous cytotrophoblast

ABSTRACT

The establishment and function of the human placenta is dependent on specialized cells called trophoblasts. Progenitor cytotrophoblasts (CTBs) differentiate along one of two cellular trajectories: the villous or extravillous pathways. CTBs committed to the villous pathway fuse with neighboring CTBs forming the outer multinucleated syncytiotrophoblast layer (SCT), while CTBs committed to the extravillous pathway develop into multi-layered cell columns that anchor the placenta to uterine tissue. At distal column sites, column CTBs differentiate into invasive extravillous trophoblasts (EVT) that facilitate uterine remodeling of spiral arteries and modulate the maternal immune response to fetal antigen. Unfortunately, little is known about the cellular and molecular processes controlling human trophoblast stem cell maintenance and differentiation into these critical trophoblast sub-lineages. To address this, our laboratory established a single cell RNA sequencing (scRNA-seq) dataset from first trimester placentas to identify molecular programs and cell states important in trophoblast progenitor establishment, renewal, and differentiation. Using this dataset, eight distinct trophoblast states were identified, representing progenitor cytotrophoblasts, intermediate column CTBs, syncytiotrophoblast progenitors, and terminally differentiated EVT. Lineage trajectory analysis identified a CTB origin that was reproduced in human trophoblast stem cell organoids. Heightened expression of basal cell adhesion molecule (*BCAM*) defined this primitive state, where CTBs selected for high levels of surface BCAM expression generated larger clonally-derived organoids than did CTB counterparts expressing lower levels of BCAM. Together, this work resolves complex gene networks within human trophoblast progenitor cells, and identifies BCAM as marker that defines an up-stream progenitor origin.

72 **INTRODUCTION**

73 The placenta is a blastocyst-derived tissue that shares the genetic identity of the developing
74 fetus. Derived from cells of the trophectoderm and extraembryonic mesoderm, the human placenta
75 matures into a functional organ by 10-12 weeks' gestation (GA)[1-3]. Through its direct interaction with
76 maternal uterine epithelial, stromal, and immune cells, the placenta coordinates the establishment of the
77 maternal-fetal-interface and serves as a critical barrier important for nutrient-waste exchange between
78 maternal and fetal circulations. Trophectoderm-derived trophoblasts perform many functions of the
79 placenta. These include, but are not limited to the facilitation of nutrient and oxygen transfer between
80 mother and fetus[4], the modulation of the maternal immune response towards the semi-allogeneic fetus
81 and placenta[5,6], and the production of hormones (i.e. chorionic gonadotropin, progesterone, placental
82 lactogen) and other factors required for pregnancy[7].

83 Of all eutherian mammals, the human placenta is the most invasive[3]. Though humans and
84 rodents both share a hemochorial arrangement of trophoblast and uterine tissue, control of uterine
85 surface epithelial and stromal erosion, as well as artery remodeling by trophoblasts during blastocyst
86 implantation and early placental establishment is far more extensive in humans than in rodents[8].
87 Importantly, key regulators of trophoblast lineage specification in rodents (i.e. *Cdx2*, *Eomes*, *Esrrb*, and
88 *Sox2*) do not appear to play essential (or identical in the case of *Cdx2*) roles in human trophoblasts[9].
89 These important differences in human trophoblast biology underlie the need to use human placentas
90 and cell systems for generating fundamental knowledge central to human trophoblast and placental
91 development. While recent advances in regenerative trophoblast culture systems have created the
92 necessary tools required for in-depth cellular and molecular understandings central to trophoblast
93 differentiation[10-12], to date, few studies have used these platforms to examine at high resolution
94 trophoblast progenitor and/or stem cell dynamics.

95 In humans, two major trophoblast differentiation pathways – villous and extravillous – give rise

to all trophoblasts in the fetal-maternal interface (Figure 1A). In the villous pathway, progenitor cytotrophoblasts (CTBs) fuse with neighboring CTBs to replenish or generate new syncytiotrophoblast (SCT), a multinucleated outer layer of the placenta that is the site of transport of most substances across the placenta, and is also the placenta's major metabolic and endocrine engine. Cells committed to differentiate along the extravillous pathway are predicted to originate from CTB progenitors proximal to anchoring villi[9], though populations of villous CTB may already be programmed towards extravillous differentiation or may alternatively harbor a level of bi-potency[2,13]. Nonetheless, progenitors devoted to this pathway give rise to extravillous trophoblasts (EVTs) that anchor the placenta to the uterine wall (i.e. proximal and distal column CTB) and these cells adopt invasive characteristics hallmarked by interstitial and endovascular EVT subsets that facilitate uterine tissue and artery remodeling, and interact with and modulate maternal immune cell activity[14-16]. Defects in trophoblast differentiation along either pathway associate with impaired placental function that may contribute to, or drive, the development of aberrant conditions of pregnancy[17].

In this study, we integrate an in-house first trimester placenta single cell RNA-sequencing (scRNA-seq) dataset (7 unique placentas) with a publicly available first trimester placenta/decidual scRNA-seq dataset consisting of 4 additional samples[18]. Using this data, we investigate trophoblast heterogeneity across the first trimester and identify a CTB origin state that likely represents a trophoblast stem cell/progenitor population. Within this upstream progenitor state, we show elevated expression of the gene *Basal Cell Adhesion Molecule* (*BCAM*), where isolation and culture of BCAM^{hi} CTBs result in robust organoid establishment and growth. Together, this work reaffirms prior findings related to CTB biology, maintenance, and renewal, and further identifies new gene pathways underlying distinct CTB progenitor/stem states upstream of SCT and EVT sub-lineage commitment that are central to placental development.

120 **RESULTS**

121 **Single cell transcriptomics resolves trophoblast heterogeneity and cell state dynamics**

122 Single-cell transcriptomic analysis enables the identification of novel cell types and cell states
123 in a systematic and quantitative manner. Here, we applied the 10X Genomics Chromium platform to
124 sequence the healthy human placental transcriptome at single cell resolution (n=7 placentas), and
125 merged this data with publicly available single-cell transcriptomic profiles of healthy human maternal-
126 fetal interface tissues (n=4 placentas, n=4 deciduas) (Figure 1B). To examine developmental
127 differences, we grouped individual samples into early (6-7 weeks') and late (9-12 weeks') gestational
128 age (GA) ranges. Clinical characteristics and sequencing metrics from each patient and sample are
129 summarized in Supplemental Tables 1 and 2. 50,790 cells remained after quality control and data pre-
130 processing (Supplemental Figure 1A-C). Principal component (PC) analysis validated data integration
131 between our placental data and the MFI data collected from ArrayExpress with separation of cells
132 explained by tissue type, not data source (Supplemental Figure 1D). These cells were clustered into 14
133 cell types and 31 distinct cell states by transcriptomic similarity (Supplemental Figure 1E). The
134 influence of fetal gestational age on placental and decidual cell composition was compared, where late
135 first trimester samples showed greater uterine cell coverage than early samples (Supplemental Figure
136 1F). All clusters were identified by comparing gene expression profiles (Supplemental Figure 1G), and
137 cell cycle phase proportions per cluster informed the level of proliferation in each cell state within the
138 first trimester (Supplemental Figure 1H). Decidual cells were identified by vimentin expression and
139 decidual immune cells were specifically identified by *PTPRC* transcripts that encode the leukocyte
140 CD45 antigen (Supplemental Figure 1I). Additional markers were used to identify endothelial, stromal,
141 and fibroblastic cell compartments of the maternal fetal interface, defining the heterogenous landscape
142 and dynamic nature of these cells (Supplemental Figure 1I).

143 For trophoblast identification, cells expressing combinations of trophoblast-related transcripts

144 (i.e. *KRT7*, *EGFR*, *TEAD4*, *TP63*, *TFAP2A*, *TFAP2C*, *GATA2*, *GATA3*, *HLA-G*, *ERVFRD-1*), and
145 lacking mesenchymal- and immune-related transcripts (i.e. *VIM*, *WARS*, *PTPRC*, *DCN*, *CD34*, *CD14*,
146 *CD86*, *CD163*, *NKG7*, *KLRD1*, *HLA-DPA1*, *HLA-DPB1*, *HLA-DRA*, *HLA-DRB1*, *HLA-DRB5*, and
147 *HLA-DQA1*), were subset for further analysis (Supplemental Figure 1G, 1J). Eight distinct trophoblast
148 clusters from 7,798 cells were resolved (Figure 1C). Within these 8 clusters, we identified four CTB
149 states (CTB1-4; *EGFR*$^+$, *ELF5*$^+$), a CTB state expressing the SCT-related genes that we termed
150 progenitor syncytiotrophoblast (SCTp; *ERVFRD-1*$^+$, *CGB*$^+$), two column trophoblast states (cCTB1-2;
151 NOTCH1$^+$, ITGA5$^+$), and a state specific to EVT (EVT; *HLA-G*$^+$, *ITGA1*$^+$) (Figure 1C, 1D;
152 Supplemental Table 3). Moreover, CTB1-4 showed varying degrees of enrichment for genes associated
153 with trophoblast progenitor/stem states (i.e. *CDX2, TP63*, *ELF5*, *TEAD4*), where CTB2 and CTB3
154 showed the greatest enrichment for progenitor genes (Figure 1D).

155 Column trophoblasts are precursors to EVT, where cells situated within proximal and distal
156 sites of anchoring columns can be molecularly distinguished by expression of distinct NOTCH and
157 integrin genes[19,20]. To this end, cCTB2 expresses high levels of *NOTCH1*, *SOX9,* and *ITGA2*, the latter
158 of which defines a distinct EVT progenitor population[13] and therefore likely represents a proximal
159 column EVT progenitor (Figure 1D). Compared to cCTB2, cells within the cCTB1 state showed higher
160 levels of *ITGA5*, *NOTCH2*, and *HLA-G*, indicating that this state is developmentally downstream of
161 cCTB2 and cells within this state likely reside within central and distal regions of anchoring columns[21]
162 (Figure 1D). Stratifying cells by phases of the cell cycle showed that cCTB1 column cells are
163 predominately in G2, M, and S phases, while cCTB2 column cells are not actively cycling (Figure 1E).
164 As expected, terminally differentiated EVT and SCTp states are largely non-cycling G1 cells, as are
165 progenitor CTB1-3 states (Figure 1E). This was in contrast to CTB4, where the vast majority of cells
166 are actively cycling and express hallmark genes linked to proliferation (i.e. *MKI67*, *CCNA2*) (Figure
167 1D-F). Importantly, these distinct trophoblast states largely align with recent single cell transcriptomic

168 characterizations of cells from first trimester pregnancies[18,22,23].

169 Having defined eight trophoblast types/states within first trimester placental villi, we next
170 examined their stability across the first trimester developmental period. Relative steady-state
171 frequencies in CTB1 and CTB3 states were observed in placentas from 6-7 weeks' and 9-12 weeks'
172 GA, whereas more dynamic changes were seen in other states (Figure 1G). The proportion of cells
173 comprising the proliferative CTB4 state decreased slightly from the early (18%) to late (11%) first
174 trimester (Figure 1G). Moderate decreases in frequency were also seen in cells within column (cCTB1,
175 cCTB2), EVT, and SCTp states (Figure 1G). This was in mark contrast to CTB2, which showed a ~3-
176 fold increase from 8% to 29% (Figure 1G). Together, these findings define unique states of trophoblast
177 heterogeneity in the early and late first trimester developmental window, a developmental period
178 correlating with an onset in maternal blood perfusion within the intervillous space around 10 weeks'
179 GA, and a significant expansion/branching of floating placental villi.

180

181 **Defining the trophoblast landscape and ordering of known and novel gene programs in CTB**
182 **progenitors**

183 With the recent development of regenerative human trophoblast models that better facilitate the
184 study of progenitor CTB differentiation into SCT and EVT, significant strides have been made in our
185 understanding of key pathways underlying CTB establishment, maintenance, and the initial molecular
186 programs driving CTB differentiation[10-12,24,25]. For example, WNT, HIPPO, and EGFR signaling are
187 essential in human trophoblast stem cell establishment[10-12], and impairments in trophoblast stem cell
188 regeneration in the context of YAP-TEAD4 complex perturbation[24,25] underscore the necessity of these
189 pathways in placental development. To examine how previously described pathways critical to CTB
190 development are altered during differentiation, we applied a simple branched pseudotime trajectory

191 analysis (using Monocle2) to order cells and states in pseudotime (Supplemental Figure 2A, 2B). We
192 focused on the transitions occurring between trophoblast cell type, and more specifically cell state, with
193 increased pseudotime maturation along either of the defined villous or extravillous trajectories
194 (Supplemental Figure 2B). While simple branched pseudotime ordering did not resolve a
195 developmental lineage within the four CTB states, a predicted cell state/type origin was identified
196 comprising cells within CTB1-4, and pseudotime ordering did delineate a transition from cCTB2 into
197 cCTB1 which further progress towards EVT (Supplemental Figure 2B). Monocle2 ordering also
198 highlighted the transition from CTB to SCTp; these findings are in line with recent pseudotime
199 ordering characterization of trophoblasts showing a defined origin and two differentiation trajectory
200 branches[18].

201 Aligning WNT, HIPPO, and EGFR pathway genes to the Monocle2 pseudotime trajectory
202 showed distinct patterns of gene expression in cells with proximity to the predicted origin, within
203 intermediate states along both the SCT and EVT differentiation pathways, as well as in terminally
204 differentiated SCTp and EVT states (Supplemental Figure 2C, 2D). In agreement with previous studies,
205 Dickkopft-1 (*DKK1*; an inhibitor of Wnt signaling), leucine-rich repeat-containing G-protein coupled
206 receptor 6 (*LGR6*; a Wnt receptor), the Wnt ligand genes *WNT5B* and *WNT5A*, the HIPPO signaling
207 genes transcriptional enhancer factor TEF-3 (*TEAD4*) and protein salvador homolog 1 (*SAV1*), and the
208 EGFR ligand betacellulin (*BTC*) are enriched within CTB cell states aligning to or proximal to the
209 predicated origin (Supplemental Figure 2C, 2D). As trophoblasts progress along the EVT pathway,
210 expression levels of specific Wnt-related genes (i.e. *AXIN2*, *WNT11*, *WNT9A*, *FZD4*) and the EGFR
211 ligand *AREG* transiently increase within intermediate cCTB states (Supplemental Figure 2C, 2D).
212 Nearing terminal EVT differentiation, the Wnt-ligand *WNT10B* markedly increases, as do specific
213 HIPPO-related transcription factors (*TEAD2*, *TEAD1*), and modulators (*FAT1*, *FAT2*, *WWTR1*), and the
214 EGFR receptor *ERBB2* (Supplemental Figure 2C, 2D). Along the villous trajectory, SCT progenitors

215 up-regulate the Wnt receptor *FZD1* and multiple Wnt ligands (*WNT2*, *WNT2B*, *WNT3A*, *WNT7A*), as
216 well as the HIPPO pathway transcription factor TEAD3 and the EGFR's *ERBB3* and *ERBB4*
217 (Supplemental Figure 2C, 2D). Together, lineage trajectory modeling and alignment of key
218 genes/pathways known to be important in CTB regeneration and differentiation provides a
219 comprehensive landscape of distinct effectors and regulators putatively controlling trophoblast
220 development in early pregnancy.

221 To resolve the genetic similarities and differences between distinct CTB states, all four CTB
222 states were subset for targeted transcriptomic analyses (Figure 2A). Next, we compared CTB1-4 using
223 the top 10 unique genes expressed in each state (Figure 2B). This approach characterized CTB1 as a
224 translationally active cell state, CTB2 as a cell state made up of more classically defined CTBs (i.e.
225 expressing *SPINT1*), CTB3 as a metabolically active state defined by mitochondrial gene enrichment,
226 and CTB4 as a proliferative state (Figure 2B). The similarities in gene expression across all four CTB
227 states revealed 944 genes upregulated within all CTBs (compared to more differentiated trophoblast
228 states), including the known CTB markers *TP63*, *EGFR*, and *TEAD4* (Figure 2D; Supplemental Table
229 4). Specific to each CTB state, we found upregulation of *PGF* in CTB1, upregulation of the
230 extracellular laminin gene *LAMC2* and the transcription factor *HOXB2* in CTB2, upregulation of
231 *GATA2*, *FZD3*, and *AXIN2* in CTB3, and upregulation of *TFAP4* and *TFAP2B* in CTB4 (Supplemental
232 Table 4). Gene ontology terms enriched from those genes uniquely upregulated in each state revealed
233 that CTB1 is involved in general metabolic processes (Figure 2E), CTB2 is involved in cell stemness
234 and general responses to hypoxia (Figure 2E), CTB3 has terms describing the suppression of
235 mitochondrial activity and promoting cell anabolism (Figure 2E), and CTB4, is involved in cell cycle
236 progression and chromosome organization/segregation (Figure 2E). Finally, *cis*-regulatory sequence
237 analysis of the enriched genes per CTB state revealed a list of 62 transcription factors (TFs) that may
238 act as CTB-specific regulators (Figure 2F). Included in this list are TFs known to be important in CTB

239 biology like *TEAD4* and *TFAP2A*[25]. Interestingly, TFs such as transcriptional regulator KAISO
240 (*ZBTB33*) involved the negative regulation of the WNT pathway[26] shows enrichment in CTB3. These
241 findings highlight the cellular and molecular complexity within the CTB compartment of the placenta,
242 and identify possible transcriptional regulators important in controlling the maintenance of progenitor
243 CTBs as well as regulating the possible transition between unique CTB states.

244

245 **Single cell trajectory modeling identifies a CTB origin**

246 RNA velocity, the time derivative of the gene expression state, can be used to predict the future
247 transcriptional state of a cell. RNA velocity analysis in combination with single-cell trajectory analyses
248 provides us with insights into the transcriptional dynamics of developing cells and enables high-
249 resolution lineage pathway ordering. By applying scVelo to our dataset to further refine progenitor and
250 cell end-point relationships, we identified CTB2 as a first trimester placental trophoblast stem cell
251 origin from which all other trophoblasts derive (Figure 3A). We identified two paths extending from
252 this origin towards the EVT state and one path developing from the origin towards the SCTp state. As
253 well, we found an additional differentiation trajectory, extending from CTB2 into CTB3, representing a
254 potential CTB progenitor reserve.

255 To more completely understand the developmental steps involved in CTB differentiation, we
256 applied complex pseudotime ordering using Monocle3. Similar to RNA velocity, CTB2 was identified
257 as the CTB origin showing increased complexity as CTBs progress along one of two trajectories that
258 lead to either EVT or SCT end-point states (Supplemental Figure 3A, 3B). Specifically, complex
259 pseudotime ordering revealed a looped trajectory within CTB2 that exits towards CTB3, SCTp, and
260 EVT states (Supplemental Figure 3C). We compared these refined trajectories with expression patterns
261 of known CTB progenitor/stem cell genes. Predominant expression of *ELF5*, *YAP1*, and *ITGA6* was

262 observed in CTB3, while expression of CTB stem cell transcription factor *CDX2* showed predominant
263 expression within the CTB2 state (Figure 3B). Because CTB2 and CTB3 shared expression of multiple
264 trophoblast progenitor genes, we examined genes both shared and unique to these states (Figure 3C).
265 Twenty-five genes were shown to overlap between CTB2 and CTB3, including the genes *EGFR, IGF2,*
266 and *FBLN1* (Figure 3C). The CTB3 progenitor state expressed 274 unique genes, and of these genes,
267 many associate with trophoblast stem cell and regenerative properties (i.e. *YAP1, TP63*), Wnt signaling
268 (*LRP5*), and cell-matrix interactions (*MMP14, MMP15, ITGA6, LAMA5, LAMB1*) (Figure 3C). The
269 predicted CTB2 origin expressed 269 unique genes, including the Wnt ligand, *WNT7A*, the laminin
270 receptor basal cell adhesion molecule (*BCAM*), and the transcriptional modulators *TFAP2A* and
271 *CITED2* (Figure 3C). The expression patterns of select genes in these CTB states over pseudotime
272 support scVelo and Monocle3 trajectory ordering suggesting that CTB2 is upstream of CTB3 (Figure
273 3D; Supplemental Figure 3C). Focusing specifically on the CTB2 origin state, we identified the
274 enrichment of *BCAM*, a gene encoding a laminin cell surface receptor (Figure 3E). Also enriched
275 within this primitive CTB2 state were the genes *SOD3*, *GPC3*, *EFEMP1*, *EPN3*, and *C10orf54* (Figure
276 3E). Cumulatively, we have identified a primitive CTB state within the first trimester placenta that
277 shows molecular features of a putative CTB stem cell population possessing a unique gene expression
278 profile that includes the early stem marker *CDX2* and the cell surface glycoprotein *BCAM*.

279

280 **Human trophoblast stem cells recapitulate scRNA-seq-informed CTB heterogeneity and**
281 **hierarchy**

282 Recently described regenerative human trophoblast models provide an improved method for
283 modeling trophoblast differentiation *in vitro*[10]. Three-dimensional organoid-like cultures of human
284 trophoblast stem cell lines (hTSCs) have also been shown to reproduce molecular features underlying

285 CTB maintenance and differentiation[25]. To examine the reproducibility of trophoblast-intrinsic
286 differentiation programs defined by scRNA-seq analysis of *in vivo* placental specimens, we subjected
287 three hTSC lines to scRNA-seq analysis prior to and following EVT-directed differentiation.
288 Regenerative and EVT differentiating hTSC organoids (i.e. CT27, CT29, and CT30 CTB lines) were
289 cultured for 7 days in regenerative Wnt^+ (containing the Wnt potentiators R-spondin and CHIR99021)
290 and EVT-differentiating Wnt^- (lacking R-spondin and CHIR99021) media, respectively, prior to single
291 cell workflow. To confirm the intactness of our model system, a separate cohort of hTSC organoids
292 were cultured over 21 days in these media and differentiation was assessed by light microscopy, flow
293 cytometry, and qPCR analysis. hTSC-derived organoids cultured in regenerative media established
294 large spherical colonies characterized in part by elevated expression of the CTB progenitor genes
295 *TEAD4* and *ITGA6* (Figure 4A, 4C). Moreover, expression of surface MHC-I (HLA-A, -B, -C) by flow
296 cytometry did not detect these MHC-I ligands in undifferentiated cultures, (Figure 4B). Comparatively,
297 hTSC organoids cultured in EVT differentiating Wnt^- media showed characteristic cellular elongations
298 and extensions from the organoid body (Figure 4A), as well as a marked decrease in levels of *TEAD4*
299 mRNA (Figure 4C). As expected, both immature (*ITGA5*, *NOTCH1*) and mature (*NOTCH2*, *HLA-G*)
300 EVT marker genes, as well as HLA-C and HLA-G surface expression increased along the EVT
301 differentiation time-line (Figure 4B, 4C), indicating that the 3D organoid model to study CTB
302 regeneration and EVT differentiation is intact.

303 13,395 regenerative and 40,572 EVT-differentiated hTSC organoid cells were then used to
304 generate single cell cDNA libraries following the 10X Genomics Chromium workflow. Combining
305 single cell transcriptomic data from CT27, CT29, and CT30 hTSC organoids resolved 7 distinct cell
306 states based on global gene expression signatures; three CTB (CTB1-3), a pre-syncytiotrophoblast
307 (SCTp), a putative column/EVT progenitor (cCTB), and two EVT-like states (EVT1, EVT2) were
308 identified (Figure 4D). Hallmark gene markers of trophoblast-lineage (*TFAP2A, TFAP2C*), CTB

309 progenitors (*TEAD4, YAP1, TP63, ITGA6, ELF5*), syncytiotrophoblast (*ERVFRD-1, ERVV-1, SDC1*),
310 immature (*ITGA5, ITGA2, NOTCH1*) and mature EVT (*ITGA1, NOTCH2, HLA-G*), as well as gene
311 markers of proliferation (*MKI67, CCNA2*) are shown corresponding to individual cell states (Figure
312 4D). CTB1-3 shared great overlap in gene expression, though CTB1 distinctly expressed proliferative
313 genes that also co-expressed at high levels the progenitor genes *TEAD4*, *TP63*, and *ELF5* (Figure 4D).
314 While CTB2 and CTB3 also expressed progenitor genes, their levels were comparatively lower than
315 levels in CTB1 (Figure 4D). The putative column/EVT progenitor state cCTB uniquely expressed
316 *ITGA2*, *SOX9*, and the immature EVT marker *NOTCH1*; at the gene level, this unique state resembles
317 the EVT progenitor population described in Lee *et al*[13], though unlike that progenitor population, this
318 state did not express high levels of proliferative genes (Figure 4D). States resembling more terminally
319 differentiated cell types showed strong enrichment for syncytial-like genes (SCTp) and EVT-associated
320 genes, with EVT1 showing the highest expression of *HLA-G* and *NOTCH2* (Figure 4D).

321 When scRNA-seq data for hTSC-derived organoids are plotted individually, overall cell state
322 complexity diminishes from 7 unique states to 5 states (Figure 4E). When comparing the three hTSCs
323 with each other, notable variances in cell states are observed (Figure 4E). While clearly defined
324 endpoint states are evident, variances defined by gene expression in CTB and cCTB states suggest that
325 the hTSC lines harbor cell differentiation kinetics that are different from each other (Figure 4E).
326 Nonetheless, within each hTSC-derived organoid, a CTB origin was revealed by estimation of RNA
327 velocity that overlapped with CTB1 (Figure 4E). When this origin was compared across each hTSC
328 line by relative gene expression, we found consistent up-regulation of the trophoblast stem cell genes
329 *TP63*, *YAP1*, and *PAGE4* compared to other states. However, we did see differences in the expression
330 of the *ELF5* stem gene between hTSCs and individual states. Expression of *ELF5* localized to the
331 origin in the CT27 hTSC line, but not within the origins of the CT29 or CT30 hTSC lines (Figure 4E).
332 Similar differences were observed for the proliferative gene markers *MKI67* and *CCNA2*, with positive

333 expression occurring in the origins of CT27 and CT30, but not in the origins of CT29 (Figure 4E).
334 When averaged across all hTSC lines, however, we observed consistent expression of *ELF5*, *BCAM*,
335 *MKI67*, and *CNNA2* within the CTB origin (Figure 4D). Comparison of transcriptional signatures
336 between the scVelo-determined origins in *in vivo* trophoblasts from chorionic villi and hTSC-derived
337 organoids highlights that there is considerable overlap between the CTB2 & 3 (*in vivo*) and CTB1& 2
338 (*in vitro*) states (Figure 4F). Notably, we show *BCAM* to be one of the most highly expressed genes
339 within primitive states identified *in vivo* and in hTSC (Figure 4G, 4H). This suggests that BCAM may
340 be a novel CTB stem cell or progenitor marker.

341

342 **BCAM-enrichment confers increased CTB regenerative potential**

343 To our knowledge, BCAM localization within the human placenta has never been reported. To
344 this end, we probed early (6.3 week) and late (11.2 week) first trimester placental villi specimens with
345 BCAM antibody (Figure 5A). A specific and strong BCAM signal was observed in CTB of both
346 developmental time-points, and serial sections stained with keratin-7 (KRT7) and HLA-G showed that
347 BCAM was present within proximal column cells, though the intensity of the signal was less than in
348 CTB (Figure 5A). Serial sections of villi stained with KRT7 and hCG clearly showed that BCAM is
349 absent from the syncytiotrophoblast outer layer (Figure 5A). In hTSC-derived organoids cultured in
350 regenerative Wnt^+ media, BCAM signal was specific to the outer CTB layer and absent within the
351 hCG^+ syncytium (Figure 5B). Dual-labeling with BCAM and Ki67 antibody in CT29 hTSC-derived
352 organoids showed that $BCAM^+$ CTB and proximal column trophoblasts also stained positive for the
353 proliferation marker (Figure 5B). Flow cytometry, which enables a quantitative measure of BCAM cell
354 frequency, showed that in dissociated $EGFR^+$ CTB from CT29-derived organoids, ~90% of CTBs are
355 BCAM positive (Figure 5C).

356 To test the regenerative potential of BCAM-expressing cells, BCAM^{hi} and BCAM^{lo} CTBs (i.e.
357 EGFR^{+} trophoblasts) were sorted from CT29 hTSC organoids and seeded as single cells at a density of
358 125 cells/μl within Matrigel domes and cultured over 11 days (Figure 5D). While the colony take-rate
359 did not differ between BCAM^{hi} and BCAM^{lo} CTB organoids (Supplemental Figure 4), BCAM^{hi}
360 organoid colony size appeared to be larger by day 7 of culture, with BCAM^{hi} colonies being
361 significantly larger than BCAM^{lo} colonies on days 9-11 in culture (Figure 5E). Notably, flow
362 cytometry assessment of endpoint day 11 BCAM^{hi} and BCAM^{lo} organoids showed that while BCAM^{hi}-
363 sorted cells retained frequencies of >90% BCAM high-expressing cells (Figure 5F), the frequency of
364 CTBs expressing BCAM in BCAM^{lo}-sorted cells was only marginally less, suggesting that the BCAM
365 phenotype is dynamic. Comparing differentially expressed genes between BCAM^{hi} and BCAM^{lo}
366 EGFR+ CTBs showed that BCAM^{hi} cells expressed higher levels of the paternally imprinted
367 transcription factors *PEG3* and *PEG10* involved in potentiating progression through the cell cycle and
368 stem cell renewal genes *EPCAM* and *HMGB3*[27] (Figure 5G). In summary, these data show that
369 enrichment of BCAM high-expressing CTB confers organoid growth and regenerative potential.

370

371

372 **DISCUSSION**

373 Here we applied single cell RNA sequencing of human placentas at two gestational age
374 timepoints within the first trimester to further our understanding of human trophoblast development. In
375 doing this, we provide here novel transcriptomic data from 7,798 human trophoblasts, resolve the first
376 trimester trophoblast landscape at increased resolution, and clarify how gestational age informs
377 trophoblast heterogeneity, composition, and gene expression. To our knowledge, this is the first
378 trophoblast-focused study that accounts for multiple gestational age timepoints within the first
379 trimester. Using state-of-the-art single cell lineage trajectory tools, we trace back the lineage
380 commitments made by developing CTBs to identify a novel trophoblast progenitor cell niche marked
381 by increased expression of the cell surface glycoprotein BCAM.

382 Previous studies have explored the maternal-fetal interface transcriptome[18] as well as the
383 placental transcriptome across gestation at single cell resolution[22,23]. While these studies have
384 contributed important insight into placental cell heterogeneity, complexity, and have defined detailed
385 maternal-trophoblast interactions, a strict focus on understanding CTB hierarchy, the CTB progenitor
386 transcription factor regulatory landscape, and gene pathways underlying CTB commitment to EVT or
387 SCT has not been specifically addressed. Our study defines four cytotrophoblast states. The first CTB
388 state is identified by increased expression of large (RPL) and small (RPS) ribosomal subunit genes.
389 Upregulation of these ribosomal subunit genes suggests increased ribosome content, and therefore
390 increased protein translation occurring within these cells[28]. Some studies have reported a link between
391 ribosomal subunit protein activity and regulation the cell cycle through P53-mediated arrest or the
392 promotion of proliferation[29]. The mixed expression of both activators (*RPS15A*[29]) and inhibitors
393 (*RPS14*[29]) of proliferation within this CTB state suggests that this cell state may represent a transient
394 CTB population increasing expression of ribosome genes to regulate entry into the cell cycle[28,29].
395 Further, previous work by Khajuria et al[30] has described a link between ribosome protein level and cell

396 differentiation, suggesting an alternative explanation that these cells are increasing expression of
397 ribosome subunits to facilitate differentiation out of the trophoblast stem cell state.

398 The second CTB state we define is a population of proliferative CTBs. Previous studies have
399 proposed that proliferating CTBs will generally contain trophoblast stem cells[23], allowing these
400 dividing cells to supply and replenish the placenta across gestation. Expression patterns of known
401 trophoblast stem cell markers, however, shows little overlap with these cells in our data, the exception
402 being *TEAD4*, which is identified as a potential key regulator of this state. Previous work has
403 demonstrated multiple roles for the TEA domain (TEAD) proteins in cell proliferation, differentiation,
404 and apoptosis[31-34]. Specifically, TEAD4 coactivation with VGLL1/2 proteins is shown to promote
405 proliferation, while TEAD4 coactivation with the Hippo pathway effector protein YAP has been
406 demonstrated to promote trophoblast stemness[24]. Comparison of the expression patterns of *TEAD4* and
407 *YAP1* (encoding the YAP protein), in our proliferative CTBs and in CTB2 suggests a dual role of
408 *TEAD4* expression in the CTB, dependent on the expression of these coactivators. Within our
409 proliferative CTBs, *TEAD4* is co-expressed with *VGLL1* without *YAP1*, demonstrating that here
410 TEAD4 is driving a proliferative and not stem phenotype.

411 The third CTB state identified is a metabolically active state, identified by increased expression
412 of mitochondria genes. Previous sequencing reports have noted that increased percent expression of
413 mitochondrial RNA may be indicative of cell stress or damage[35-37]. However, our quality control
414 pipeline filters on the basis of percent mitochondrial RNA content. As well, comparison of cell specific
415 feature detection and the detection of unique molecular identifiers indicates no observable difference
416 that would support the presence of damaged or dying cells. As a result, we theorize that these cells are
417 expressing mitochondrial RNA transcripts in response to increased metabolic demand. Unique to this
418 CTB state is the upregulation of many genes shown to be involved in trophoblast stemness, suggesting
419 a role for mitochondrial activity in CTB stemness. Fitting with this, recent work has shown a direct role

420 for WNT signaling in the promotion of CTB stemness[10-12], suggesting that these cells, which express a
421 CTB progenitor-like transcriptome but are not the CTB progenitors, may represent a transient CTB
422 state responding to WNT activation. To further support this hypothesis, recent work has demonstrated a
423 correlation between WNT activity and mitochondrial biogenesis/activation[38,39], however further work
424 is needed to test this in the placenta. Interestingly, three transcription factors were identified as master
425 regulators of this CTB state, ZBTB33, TFCP2L1, and FOXK1, all of which show involvement in the
426 regulation of WNT signaling.

427 We then sought to identify and characterize a trophoblast stem cell niche. Our initial approaches
428 involved branched pseudotime trajectory inference, which captured transitions between cell type as
429 CTB differentiate into SCT or EVT, however, this approach proved insufficient for delineating the
430 CTB specific developmental hierarchy. To circumvent this and identify the most primitive trophoblast
431 population, we applied a sophisticated RNA velocity approach for quantifying the relative amounts of
432 spliced and unspliced gene abundances. RNA velocity was able to identify CTB2, the fourth state, as
433 an origin population from which all trophoblasts arise. Within these cells, we observe increased
434 expression of the most primitive trophoblast stem cell gene *CDX2*, further indicating that these cells
435 represent a primitive CTB state. Gene ontology enrichment analysis of genes in CTB2 identified
436 biological process terms relating to hematopoietic progenitor cell differentiation and cellular response
437 to hypoxia. The first 9 weeks of gestation are characterized by a hypoxic oxygen concentration < 20
438 mm Hg that is maintained until maternal trophoblastic plugs are eroded at 10 weeks GA, bringing the
439 oxygen concentration of the maternal fetal interface to 40-80 mmHg[40-43]. Enrichment of hypoxia cell-
440 related terms within this origin indicates that these cells are highly sensitive to their environment, but
441 also that hypoxia-driven programs may play roles in coordinating progenitor functions in CTB. Indeed,
442 exposure to low levels of oxygen drive CTBs to differentiate into immature EVT[44-46], but the
443 contribution of hypoxia on progenitor biology is not as well developed. Future work aimed at

444 understanding the relationship between hypoxia and stemness in trophoblast development, including
445 the importance of HIF transcription factors in stem cell maintenance will be important.

446 Comparisons between our placental tissue sequencing data and our trophoblast organoid
447 sequencing data demonstrate similarities in general CTB, SCT and EVT function, but also subtle
448 differences between the different states of CTB found in each stem cell derived organoid condition and
449 our tissue CTBs. Comparison of the CTB progenitor niche identified in both the organoid and tissue
450 datasets identifies the common transcription factors *YAP1*, *SPINT2*, *PEG10*, and *MSI1* as well as
451 consistent upregulation of *BCAM*, supporting identification of BCAM as a CTB progenitor marker.
452 Interestingly, quantification of mRNA levels of known CTB related genes (*TEAD4* and *ITGA6*) as well
453 as SCT (*CGB* and *CSH1*) and EVT related genes (*ITGA5*, *NOTCH1*, *NOTCH2*, and *HLA-G*) on days 0,
454 11, and 21 of differentiation indicate that hTSC specific organoid colonies show different rates of
455 differentiation or capacities to differentiate. Our EVT-differentiated organoid transcriptomes were
456 sequenced on day 7 of differentiation, indicating that the differences we are observing may in part be
457 due to groups of organoid colonies being at a different stage of differentiation, with CT29 derived
458 organoids showing the most rapid capacity for EVT differentiation, followed by CT30 and CT27.

459 Consistent between our *in vivo* and *in vitro* datasets is the identification of two cytotrophoblast
460 progenitor cell niches in the first trimester placenta, one representing a CTB origin state marked by
461 increased *BCAM* gene expression, and one representing a more specified bipotent EVT progenitor cell
462 state, marked by *ITGA2* and *NOTCH1* gene expression. Immunofluorescence microscopy and
463 immunohistochemistry of 8-9 week gestationally aged placental villi has previously demonstrated that
464 ITGA2 is specific to proximal cells within anchoring placental villi, near the basement membrane[13]. It
465 is thought that as chorionic villi develop early in gestation, trophoblast progenitors located within close
466 proximity to uterine stroma adapt a unique gene expression profile coinciding with the formation of
467 anchoring columns and into mature EVT. We show that the transcriptome of these putative column

468 progenitors express EVT-like *NOTCH1* and *ITGA5* and CTB-like *TFAP2C*, *GATA3*, and *ELF5*
469 transcripts. Lee et al[13] further describe ITGA2^{+} cCTBs as having a mixed endothelial- and
470 mesenchymal-like identity. This unique gene signature, harboring stem-like and EVT-like genes,
471 supports the possibility that these cells retain a level of bipotency. Analyses using scVelo trajectory
472 inference suggests these column/EVT progenitors are likely adapted from the initial BCAM^{+} CTB
473 progenitor cell niche and maintained as a reserve population within the anchoring column across the
474 first trimester.

475 Importantly, we identify specific upregulation of the Ig superfamily membrane bound
476 glycoprotein BCAM in our CTB progenitor cells. BCAM is known to interact through its ligand
477 *LAMA5*, a component of the laminin-511 heterotrimer found within the placental extracellular
478 matrix[47,48]. BCAM was identified as an antigen upregulated in ovarian carcinoma, and has been
479 described to facilitate tumor migration by competing for laminin binding with integrins in the basement
480 membrane, as well as cell-cell adhesion[49,50], designating *BCAM* as an important oncogene[51]. Here, flow
481 cytometric sorting of BCAM^{hi} and BCAM^{lo} CTBs for organoid colony formation demonstrates that
482 BCAM^{hi} cells have a significantly improved capacity for trophoblast organoid growth. Interestingly, no
483 differences were observed in the capacity of BCAM^{hi} and BCAM^{lo} CTBs to form organoid colonies,
484 suggesting that increased BCAM expression may not confer cytotrophoblast stemness. Rather, BCAM
485 expression may provide cytotrophoblast growth advantages either through a cell survival signal or by
486 increasing CTB proliferation. However, differential gene expression of CT29-derived organoid
487 BCAM^{hi} and BCAM^{lo} CTBs shows upregulation of *LRPAPR1*, *PEG10*, *SPINT2*, *EPCAM*, *LAMB1*,
488 *PDLIM1*, and *HMGB3*, indicating that BCAM may confer increased organoid growth via cytoskeleton-
489 extracellular matrix interactions or by conferring increased stemness. Interestingly, previous work has
490 demonstrated that BCAM is capable of reorganizing the red blood cell actin cytoskeleton[52], suggesting
491 BCAM activity may reorganize the CTB progenitor cytoskeleton. On day eleven of colony formation

492 we see an adoption of BCAM expression in the organoids established from BCAM^{lo} CTBs, indicating
493 that there is an upregulation of BCAM expression over time within our trophoblast organoid model.
494 Comparing the growth kinetics of BCAM^{hi} versus BCAM^{lo} organoids, this dynamic gain of BCAM
495 expression may explain the catch up in organoid size observed in BCAM^{lo} organoids on days 9-11 of
496 colony formation. The role for BCAM interaction with laminin cannot be ignored here as well, as this
497 interaction may establish an extracellular matrix progenitor cell niche. Laminin has been shown to be
498 necessary for proper trophoblast implantation, placental perfusion, and angiogenesis[53]. The inclusion of
499 laminin in Matrigel used in organoid culture may provide signaling through integrins expressed on the
500 cytotrophoblast cell surface to induce BCAM expression, explaining this observation in our BCAM^{lo}
501 organoids. Further work is necessary to decipher the exact functional role of BCAM expression and the
502 BCAM-Laminin interaction *in vivo* cytotrophoblast progenitor cells, and how this in turn facilitates
503 improved organoid growth *in vitro*.
504

505 **SIGNIFICANCE**

506 The identification of a novel cell surface human cytotrophoblast progenitor cell marker provides
507 improved methods for isolating and studying the mechanisms regulating human CTB progenitor cells,
508 trophoblast differentiation, and human placental development.
509

510 **CONCLUSIONS**

511 In conclusion, we have used single cell RNA sequencing to define trophoblast differentiation
512 trajectories in early human placental development. Importantly, we identify BCAM as a new CTB
513 progenitor marker that confers enhanced clonal growth. Future work is needed to clarify how increased
514 BCAM expression facilitates improved CTB growth, and the exact molecular paths through which this
515 occurs. We hope that future experiments will be able to capitalize on the identification of BCAM as a

516 cell surface CTB progenitor marker through which these cells can be isolated and further studied.

517

518 **MATERIALS AND METHODS**

519 **Patient recruitment and tissue collection**

520 Decidual and placental tissues were obtained with approval from the Research Ethics Board on
521 the use of human subjects, University of British Columbia (H13-00640). All samples were collected
522 from women (19 to 39 years of age) providing written informed consent undergoing elective
523 terminations of pregnancy at British Columbia's Women's Hospital, Vancouver, Canada. First
524 trimester placental tissues (*N*=7) were collected from participating women (gestational ages ranging
525 from 5–12 weeks) having confirmed viable pregnancies by ultrasound-measured fetal heartbeat. Patient
526 clinical characteristics i.e. height and weight were additionally obtained to calculate body mass index
527 (BMI: kg/m^2) and all consenting women provided self-reported information via questionnaire to having
528 first hand exposure to cigarette smoke or taken anti-inflammation or anti-hypertensive medications
529 during pregnancy. Patient and sample phenotype metadata are summarized in Supplemental Table 1.

530

531 **Human trophoblast organoids**

532 *Establishment and culture*: Human trophoblast stem cells (hTSC) CT27 (RCB4936), CT29
533 (RCB4937), and CT30 (RCB4938) from Riken BRC Cell Bank, were established from first–trimester
534 CTBs by Okae et al[10] and used here to generate organoid cultures using a modification of previously
535 described protocols[11,12]. In summary, these cells were re-suspended in ice-cold growth factor-reduced
536 Matrigel (GFR-M, Corning) to a final concentration of 100%. Cell suspensions (40µl) containing 5-20
537 x 10^3 cells were carefully seeded in the center of each well of a 24-well plate. Plates were placed at
538 37°C for 2 minutes. Following this, the plates were turned upside down to promote equal spreading of
539 the cells throughout the Matrigel domes. After 15 minutes, the plates were flipped back to normal and
540 the Matrigel domes were overlaid with 0.5mL pre-warmed trophoblast organoid media containing
541 advanced DMEM/F12 (Gibco), 10mM HEPES, 1 x B27 (Gibco), 1 x N2 (Gibco), 2mM L-glutamine

542 (Gibco), 100µg/ml Primocin (Invivogen), 100ng/mL R-spondin (PeproTech), 1µM A83-01 (Tocris),
543 100ng/mL rhEGF (PeproTech), 3µM CHIR99021 (Tocris), and 2µM Y-27632 (EMD Millipore).
544 Organoids were cultured for 7-21 days.

545 *EVT Differentiation*: EVT differentiation of trophoblast organoids was performed using an
546 adapted of previously published protocols[10]. In summary, organoids were cultured until > 50% colonies
547 reached at least 100µm in diameter (~3-5 days). Following this, organoids were maintained in EVT
548 differentiation media containing advanced DMEM/F12, 0.1mM 2-mercaptoethanol (Gibco), 0.5%
549 penicillin/streptomycin (Gibco), 0.3% BSA (Sigma Aldrich), 1% ITS-X supplement (Gibco),
550 100ng/mL NRG1 (Cell Signaling Technology), 7.5µM A83-01 (Tocris), 4% Knockout Serum
551 Replacement (Gibco). Media exchanged for EVT differentiation media lacking NRG1 around day 7-10
552 of differentiation following the visible outgrowth of cells. Differentiation was stopped at day 7 (D7) for
553 10X single cell RNA sequencing and flow cytometry analysis. Differentiation was stopped at day 21
554 (D21) for qPCR analysis.

555

556 **Placental tissue and trophoblast organoid single cell RNA-seq library construction**

557 *Placental tissue:* Healthy placental villi (BMI < 25.00 kg/m^2, MA: 20-32 years, and no
558 exposure to first hand cigarette smoke or anti-inflammation and anti-hypertensive medications during
559 pregnancy) were physically scraped form chorionic membrane by scalpel and enzymatically digested in
560 0.5ml collagenase/hyaluronidase and 1.5ml DMEM/F12 with 500µl penicillin/streptomycin and 500µl
561 100X antibiotic/antimycotic at 37˚C for 45 minutes. Placental villi cell suspensions were diluted in 1X
562 Hank's Balanced Salt Solution (HBSS) containing 2% FBS, pelleted at 1200rpm for 5 minutes, and
563 resuspended in 0.25% trypsin-EDTA. The solution was diluted again in 1X HBSS containing 2% FBS,
564 pelleted at 1200rpm for 5 minutes, and resuspended in dispase and 1mg/ml DNase I. 1X Hank's
565 Balanced Salt Solution (HBSS) containing 2% FBS was added once more and the solution was sieved

566 through a 40μm filter.

567 *Trophoblast organoids:* For all organoid cultures, media was aspirated and organoids were
568 diluted in Cell Recovery Solution at 4˚C for 40 minutes on either culture day 0 in complete media (for
569 non-differentiated organoids) or culture day 7 in differentiation media (for EVT-differentiated
570 organoids). Cells were then washed with cold PBS and centrifuged at 1000rpm for 5 minutes. Cells
571 were disaggregated in TrypLE containing 5% DNase I at 37˚C for 7 minutes before the addition of
572 100μl complete media. The resulting cell suspension was then sieved through a 40μm filter.

573 *Library construction*: Single cell suspensions (tissue- and organoid-derived) were stained with
574 7-Aminoactinomycin D (7-AAD) viability marker and live/dead sorted using a Becton Dickinson (BD)
575 FACS Aria. Cell suspensions were loaded onto the 10X Genomics single cell controller for library
576 preparation. Placental villi-derived single cell suspensions were prepared using the chromium single
577 cell 3' reagent v2 chemistry kit, following standard manufacturer protocol for all steps. Non-
578 differentiated and differentiated trophoblast organoid-derived single cell suspensions were prepared
579 using the chromium single cell 3' reagent v3 chemistry kit, following standard manufacturer protocol
580 for all steps. Single cell libraries were sequenced on an Illumina Nextseq 500 instrument at a
581 sequencing depth of 50,000 reads/cell for tissue-derived cells and 150,000 reads/cell for organoid-
582 derived cells. For placental villus samples, the 10X Genomics Cell Ranger version 2.0 software was
583 used for STAR read alignment and counting against the provided GRCh38 reference while the
584 trophoblast organoid samples used the 10X Genomics Cell Ranger version 3.0 software for STAR read
585 alignment and counting against the GRCh38 reference.

586 *Data Repository Integration*: Droplet-based first trimester scRNA-seq decidual and placental
587 tissue data was obtained from the public repository ArrayExpress (available at: E-MTAB-6701[18]). Raw
588 BAM files were downloaded and pre-processed using 10X Genomics Cell Ranger version 2.0 under
589 identical parameters as previously described for our placental villi and trophoblast organoid samples

590 using the GRCh38 reference. Sample specific metrics are summarized in Supplemental Table 2.

591

592 **Single cell RNA-seq data analysis**

593 *Data pre-processing and quality control*: A total of 50,790 single cells were sequenced and pre-
594 processed using the Seurat R package[54,55]. To ensure quality cells were used in downstream analyses,
595 cells containing fewer than 1000 detected genes and greater than 20% mitochondrial DNA content
596 were removed. Individual samples were scored based on expression of G2/M and S phase cell cycle
597 gene markers, scaled, normalized, and contaminating cell doublets were removed using the
598 DoubletFinder package[56] with default parameters and a doublet formation rate estimated from the
599 number of captured cells. Following pre-processing, all samples were merged and integrated using cell
600 pairwise correspondences between single cells across sequencing batches. During integration, the
601 Pearson residuals obtained from the default regularized negative binomial model were re-computed and
602 scaled to remove latent variation in percent mitochondrial DNA content as well as latent variation
603 resulting from the difference between the G2M and S phase cell cycle scores.

604 *Cell clustering, identification, and trophoblast sub-setting*: Cell clustering was accomplished in
605 Seurat at a resolution of 0.90 using 50 principal components. Cell identity was determined through
606 observation of known gene markers found within the maternal fetal interface (vimentin, CD45, neural
607 cell adhesion molecule, CD14, etc.) and identifying cluster marker genes via the "FindAllMarkers"
608 function using a model-based analysis of single-cell transcriptomics (MAST[57]) GLM-framework
609 implemented in Seurat. Gene markers were selected as genes with a minimum log fold change value >
610 0.20 and an adjusted p-value < 0.05 within a specific cluster. Trophoblasts were identified as
611 expressing *KRT7, EGFR, TEAD4, TP63, TFAP2A, TFAP2C, GATA2, GATA3, HLA-G, ERVFRD-1*
612 transcripts at a level greater than zero, and *VIM, WARS, PTPRC, DCN, CD34, CD14, CD86, CD163,*
613 *NKG7, KLRD1, HLA-DPA1, HLA-DPB1, HLA-DRA, HLA-DRB1, HLA-DRB5, HLA-DQA1* transcripts

614 at a level equal to zero. Trophoblasts were subset and re-clustered in Seurat at a resolution of 0.375
615 using 30 principal components. As mentioned previously, trophoblast cluster identity was determined
616 through observation of known trophoblast gene marker expression, proliferative gene marker
617 expression, and from unique cluster genes identified by differential expression analysis in Seurat.
618 Trophoblast projections were visualized using Uniform Manifold Approximation and Projections
619 (UMAPs).

620 *Differential gene expression*: Differential expression (DEG) analyses were performed in Seurat
621 using the "FindMarkers" function using a MAST framework on the raw count data. Parameters were
622 limited to genes with a log fold-change difference between groups of 0.20 and genes detected in a
623 minimum 10% cells in each group. Results were filtered for positive gene markers and significant
624 DEGs were taken as having a fold change difference > 0.25 and an adjusted p value < 0.05.

625 *Gene set enrichment analysis*: GSEA analyses were performed in Seurat using the
626 "FindMarkers" function using a MAST framework on the raw count data. Parameters included a
627 minimum log fold-change difference between groups of "−INF", a minimum gene detection of "−INF"
628 in cells in each group, and a minimum difference in the fraction of detected genes within each group of
629 "−INF", allowing all genes to be compared. Results were visualized using the R package
630 EnhancedVolcano (version 1.8.0), with a fold-change cut-off of 0.25 and a p value cut off of 0.00005
631 taken as the thresholds for significance.

632 *Gene ontology*: GO analysis of significant differentially expressed genes was performed using
633 the clusterProfiler R package[58] and the top enriched terms (Benjamini-Hochberg corrected p value
634 <0.05) were visualized as dot plots using the R package enrich plot (version 1.10.2).

635 *CTB gene regulatory network establishment*: Placental CTBs were subset and state-specific CTB gene
636 markers were identified as described in the *Differential gene expression* section, above. Results were
637 exported as an excel file for import into Cytoscape (version 3.7.1). State-specific, as well as aggregated

638 general CTB gene marker lists were imported as networks and the iRegulon package[59] was applied
639 using default parameters to define CTB gene regulatory networks.

640 *Pseudotime:* The Monocle2 R package[60-62] was used to explore the differentiation of progenitor
641 CTBs into specialized SCT and EVT. The trophoblast cell raw counts were loaded into Monocle2 for
642 semi-supervised single cell ordering in pseudotime, taking increased *BCAM* expression to represent
643 cells at the origin and *HLA-G* and *ERVFRD-1* gene expression to indicate progress towards EVT and
644 SCT, respectively. Branched expression analysis modelling (BEAM) was applied to observe the
645 expression of identified trophoblast cluster gene markers and genes related to the WNT, HIPPO,
646 NOTCH, and EGFR signaling pathways over pseudotime, progressing towards either EVT or SCT.
647 Results were visualized using the "plot_cell_trajectory" function. To resolve cytotrophoblast
648 differentiation trajectories at higher resolution, the Monocle3 package[63] was utilized. Trophoblast raw
649 counts were input, clustered, and the principal graph was created using the "learn_graph" function. The
650 "order_cells" function was then used to order cells in pseudotime, designating the trophoblast root
651 within the CTB 2 state.

652 *Lineage Trajectory*: The Velocyto package[64] was run in terminal using the command line
653 interface to generate sample-specific files containing count matrices of unspliced, spliced, and
654 ambiguous RNA transcript abundances. The velocyto.R implementation of the package was then used
655 to merge each file with its corresponding 10X sample during data pre-processing in Seurat. The final,
656 processed trophoblast object and UMAP embeddings were exported to a Jupyter Notebook and the
657 scVelo Python package[65] was used to read, prepare, and recover holistic trophoblast gene splicing
658 kinetics. Velocities were projected on top of the extracted UMAP embeddings generated in Seurat.

659 *Signaling Entropy*: The SCENT R package[66] was applied using default parameters and the
660 CCAT method for potency estimation to quantify the degree of differentiation potency and gene
661 expression promiscuity across single cells.

662

663 **Flow cytometry analysis and cell sorting**

664 *Organoid single cell work-flow*: Single cells from CT29 organoids were isolated by incubation
665 with Cell Recovery Solution (Corning) for 40 minutes at 4°C. Then, cells were washed in ice-cold PBS
666 and dissociated into single cells using TrypLE^{TM} supplemented with 5% DNAse I for 7 minutes at
667 37°C.

668 *Phenotyping EVT differentiated CT27, CT29, and CT30 organoids*: Following single cell
669 dissociation, organoid cells were stained with EGFR BV605 (clone AY13; 1:50; Biolegend), HLA-G
670 APC (clone MEMG-9; 1:50; Abcam), HLA-ABC Pacific Blue (clone W6/32; 1:100; Biolegend),
671 CD49e/ITGA5 PeCy7 (clone eBioGoH3; 1:200; Thermo Fisher Scientific), CD49f/ITGA6 Alexa 488
672 (clone P1D6; 1:200; Thermo Fisher Scientific), and BCAM BV711 (clone B64; 1:50; BD Biosciences).

673 *Phenotyping BCAM^{hi} and BCAM^{lo} organoids*: Single cells were incubated with anti-human
674 BCAM BV421 (clone B64; 1:50; BD Biosciences), EGFR BV605, and CD49f/ITGA6 PeCy7 for 30
675 minutes in the dark on ice, followed by viability staining with 7-AAD. Samples were analyzed using
676 LSRII (Becton Dickinson) and a minimum of 20,000 events were acquired.

677 *hTSC BCAM$^{hi/lo}$ sorting:* CT29 hTSCs were dissociated using TrypLE^{TM} (Thermo Fisher
678 Scientific) with 5% DNAse I (Sigma Aldrich) for 7 minutes at 37°C. Following resuspension in PBS
679 supplemented with Antibiotic-Antimycotic (Gibco) and 1% P/S (Sigma Aldrich), cells were stained
680 with BCAM BV421 (clone B64; 1:50; BD Biosciences) and EGFR Pecy7 (clone AY13; 1:50;
681 Biolegend) for 30 minutes at 4°C in the dark, followed by incubation with 7-AAD (Thermo Fisher) for
682 viability assessment. CT29 BCAM^{hi} and BCAM^{lo} populations were sorted using a FACS Aria (BD
683 Biosciences).

684

685

686 **Trophoblast organoid growth assay**

687 CT29 sorted BCAM^{hi} and BCAM^{lo} cells were seeded at a density of 5,000 cells in 40μL of
688 Matrigel in the presence of trophoblast organoid media. Phase contrast images were taken with
689 AxioObserver inverted microscope (Carl Zeiss) using 20X objective, and organoids were further
690 analyzed by qPCR, immunofluorescence, and flow cytometry. Organoid formation efficiency was
691 assessed by measuring organoid number and size (area in μm^2). Images were taken daily and analyzed
692 using imageJ (NIH). The scale was set by measuring the scale bar in pixels (285.5 pixels = 200μm).

693

694 **RNA isolation**

695 Prior to RNA extraction, organoids were dissociated into single cells as described above. Total
696 RNA was prepared from these cells using RiboZol reagent (VWR Life Science) followed by RNeasy
697 Mini kit (Qiagen) according to manufacturer's protocol. RNA purity was confirmed using a NanoDrop
698 Spectrophotometer (Thermo Fisher Scientific).

699

700 **cDNA synthesis and qPCR**

701 RNA was reverse transcribed using qScript cDNA SuperMix synthesis kit (Quanta Biosciences)
702 and subjected to qPCR (ΔΔCT) analysis, using PowerUP SYBR Green Master Mix (Thermo Fisher
703 Scientific) on a StepOnePlus Real-Time PCR System (Thermo Fisher Scientific) and forward and
704 reverse primer sets for *TEAD4* (F: 5'-CGGCACCATTACCTCCAACG-3'; R: 5'-
705 CTGCGTCATTGTCGATGGGC-3'), *ITGA6* (F: 5'-CACTCGGGAGGACAACGTGA-3'; R: 5'-
706 ACAGCCCTCCCGTTCTGTTG-3'), *CGB* (F: 5'-GCCTCATCCTTGGCGCTAGA-3'; R: 5'-
707 TATACCTCGGGGTTGTGGGG-3'), *CSH1* (F: 5'-GACTGGGCAGATCCTCAAGCA-3'; R: 5'-
708 CCATGCGCAGGAATGTCTCG-3'), *ITGA5* (F: 5'-GGGTCGGGGGCTTCAACTTA-3'; R: 5'-
709 ACACTGACCCCGTCTGTTCC-3'), *HLA-G* (F: 5'-CCCACGCACAGACTGACAGA-3'; R: 5'-

710 AGGTCGCAGCCAATCATCCA-3'), *NOTCH1* (F: 5'-GCCTGAATGGCGGGAAGTGT-3'; R: 5'-
711 TAGTCTGCCACGCCTCTGC-3'), *NOTCH2* (F: 5'-ACTCGGGGCCTACTCTGTGA-3'; R: 5'-
712 TGTCTCCCTCACAACGCTCC-3'), *GAPDH* (F: 5'-AGGGCTGCTTTTAACTCTGGT-3' R: 5'-
713 CCCCACTTGATTTTGGAGGGA-3'). All raw data were analyzed using StepOne Software v2.3
714 (Thermo Fisher Scientific). The threshold cycle values were used to calculate relative gene expression
715 levels. Values were normalized to endogenous *GAPDH* transcripts.
716
717 **Immunofluorescence microscopy**
718 Placental villi (6-12 weeks' gestation; n=2) were fixed in 2% paraformaldehyde overnight at 4
719 °C. Tissues were paraffin embedded and sectioned at 6 μm onto glass slides. Immunofluorescence was
720 performed as previously described (Aghababaei et al., 2015). Briefly, organoids or placental tissues
721 underwent antigen retrieval by heating slides in a microwave for 5 X 2 minute intervals in citrate buffer
722 (pH 6.0). Sections were incubated with sodium borohydride for 5 minutes at room temperature (RT),
723 followed by Triton X-100 permeabilization for 5 minutes, RT. Slides were blocked in 5% normal goat
724 serum/0.1% saponin for 1hr, RT, and incubated with combinations of the indicated antibodies
725 overnight at 4 °C: mouse monoclonal anti-HLA-G (clone 4H84; 1:100; Exbio, Vestec, Czech
726 Republic); rabbit monoclonal anti-cytokeratin 7 (clone SP52; 1:50; Ventana Medical Systems), rabbit
727 polyclonal anti-BCAM (1:100; Abcam); mouse monoclonal anti-hCG beta (clone 5H4-E2; 1:100;
728 Abcam). Following overnight incubation, sections and coverslips were washed with PBS and incubated
729 with Alexa Fluor goat anti-rabbit 568 and goat anti-mouse 488 conjugated secondary antibodies (Life
730 Technologies, Carlsbad, CA) for 1h at RT, washed in PBS and mounted using ProLong Gold mounting
731 media containing DAPI (Life Technologies).
732 Slides were imaged with an AxioObserver inverted microscope (Car Zeiss, Jena, Germany)
733 using 20X Plan-Apochromat/0.80NA or 40X Plan-Apochromat oil/1.4NA objectives (Carl Zeiss). An

734 ApoTome .2 structured illumination device (Carl Zeiss) set at full Z-stack mode and 5 phase images
735 was used for image acquisition.
736
737 **Statistical analysis**
738 Data are reported as median values with standard deviations. All calculations were carried out
739 using GraphPad Prism software (San Diego, CA). For single comparisons, Mann-Whitney non-
740 parametric unpaired t-tests were performed. For multiple comparisons, one-way Kruskal-Wallis
741 ANOVA followed by Dunn's multiple comparison test was performed. One-way ANOVA followed by
742 Tukey post-test were performed for all other multiple comparisons. The differences were accepted as
743 significant at $P < 0.05$. For scRNA-seq statistical analyses, please refer to scRNA-seq analysis sections
744 in methods.
745
746

747 **DATA AVAILABILITY/ACCESSION NUMBER**

748 The ArrayExpress accession number for the publicly available data reported in this paper is: E-
749 MTAB-6701.

750

751 **AUTHOR CONTRIBUTIONS**

752 AGB designed the research. AGB, MS, JB, BC, JW, SY, JT, and HTL performed experiments
753 and analysed data. AGB, MS, JB, and BC wrote the paper. All authors read and approved the
754 manuscript.

755

756 **FUNDING**

757 This work was supported by a Natural Sciences and Engineering Research Council of Canada
758 (NSERC; RGPIN-2014-04466) Discovery Grant (to AGB), Canadian Institutes of Health Research
759 201809PJT-407571-CIA-CAAA) operating grants to AGB, and a CIHR Master's graduate studentship
760 (to MS).

761

762 **ACKNOWLEDGEMENTS**

763 The authors extend their sincere gratitude to the hard work of staff at British Columbia's
764 Women's Hospital's CARE Program for recruiting participants to our study and the staff at the
765 University of British Columbia Biomedical Research Centre for assistance with all drop-seq library
766 preparation and sequencing.

767

768 **COMPETING INTERESTS**

769 The authors declare that no competing interests exist.

770

771 **REFERENCES**

772 **1.** Lee CQE, et al. What is a trophoblast? A combination of criteria define human first-trimester
773 trophoblast. *Stem Cell Reports*. 2016. 6(2): 257-272. Doi: 10.1016/j.stemcr.2016.01.006.
774 **2.** Chang CW, et al. Trophoblast lineage specification, differentiation, and their regulation by oxygen
775 tension. *J Endocrinol*. 2018. 236(1): R43-56. Doi: https://doi.org/10.1530/JOE-17-0402.
776 **3.** Pjinenborg R, et al. Deep placentation. *Best Pract Res Clin Obstet Gynaecol*. 2011. 25(3): 273-285.
777 Doi: 10.1016/j.bpobgyn.2010.10.009.
778 **4.** Burton GJ, et al. Review Histotrophic nutrition and the placental-endometrial dialogue during
779 human early pregnancy. *Placenta*. 2020 102: 21-26. Doi: 10.1016/j.placenta.2020.02.008.
780 **5.** Tilburgs T, et al. Human HLA-G+ extravillous trophoblasts: Immune-activating cells that interact
781 with decidual leukocytes. *Proc Natl Acad Sci USA*. 2015. 112(23): 7219-7224. Doi:
782 10.1073/pnas.1507977112.
783 **6.** Turco MY and Moffett A. Development of the human placenta. *Development*. 2019. 146(22):
784 dev163428. Doi: 10.1242/dev.163428.
785 **7.** Fowden AL, et al. Review: Endocrine regulation of placental phenotype. *Placenta*. 2015. 36 Suppl
786 1: S50-59. Doi: 10.1016/j.placenta.2014.11.018.
787 **8.** Geusens N, et al. Endovascular trophoblast invasion, spiral artery remodelling and uteroplacental
788 haemodynamics in a transgenic rat model of pre-eclampsia. *Placenta*. 2008. 29(7): 614-623. Doi:
789 10.1016/j.placenta.2008.04.005.
790 **9.** Knöfler M, et al. Human placenta and trophoblast development: key molecular mechanisms and
791 model systems. *Cell Mol Life Sci*. 2019. 76(18): 3479-3496. Doi: 10.1007/s00018-019-03104-6.
792 **10.** Okae, et al. Derivation of Human Trophoblast Stem Cells. *Cell Stem Cell*. 2018. 22(1): 50-63.e6.
793 Doi: 10.1016/j.stem.2017.11.004.
794 **11.** Haider S, et al. Self-Renewing Trophoblast Organoids Recapitulate the Developmental Program of
795 the Early Human Placenta. *Stem Cell Reports*. 2018. 11(2): 537-551. Doi:
796 10.1016/j.stemcr.2018.07.004.
797 **12.** Turco MY, et al. Trophoblast organoids as a model for maternal-fetal interactions during human
798 placentation. *Nature*. 2018. 564(7735): 263-267. Doi: 10.1038/s41586-018-0753-3.
799 **13.** Lee CQE, et al. Integrin α2 marks a niche of trophoblast progenitor cells in first trimester human
800 placenta. *Development*. 2018. 145(16): dev162305. Doi: 10.1242/dev.162305.
801 **14.** Pollheimer J, et al. Regulation of Placental Extravillous Trophoblasts by the Maternal Uterine
802 Environment. *Front Immunol*. 2018. 9: 2597. Doi: 10.3389/fimmu.2018.02597.

803 **15.** Papuchova H, et al. Three types of HLA-G+ extravillous trophoblasts that have distinct immune
804 regulatory properties. *Proc Natl Acad Sci USA*. 2020. 117(27): 15772-15777. Doi:
805 10.1073/pnas.2000484117.
806 **16.** Moffett A, et al. Maternal allo-recognition of the fetus. *Fertil Steril*. 2017 107(6): 1269-1272. Doi:
807 10.1016/j.fertnstert.2017.05.001.
808 **17.** Jauniaux E, et al. Placental Implantation Disorders. *Obstet Gynecol Clin North Am*. 2020. 47(1):
809 117-132. Doi: 10.1016/j.ogc.2019.10.002.
810 **18.** Vento-Tormo R, et al. Single-cell reconstruction of the early maternal-fetal interface in humans.
811 *Nature*. 2018. 563 (7731): 347-353. Doi: 10.1038/s41586-018-0698-6.
812 **19.** Haider S, et al. Notch1 controls development of the extravillous trophoblast lineage in the human
813 placenta. *Proc Natl Acad Sci USA*. 2016. 113(48): E7710-E7719. Doi: 10.1073/pnas.1612335113.
814 **20.** Zhou Y, et al. Human cytotrophoblasts adopt a vascular phenotype as they differentiate. A strategy
815 for successful endovascular invasion? *J Clin Invest*. 1997. 99(9): 2139-2151. Doi:
816 10.1172/JCI119387.
817 **21.** Haider S, et al. Notch signaling plays a critical role in motility and differentiation of human first-
818 trimester cytotrophoblasts. *Endocrinology*. 2014. 155(1): 263-74. Doi: 10.1210/en.2013-1455.
819 **22.** Suryawanshi H, et al. A single-cell survey of the human first-trimester placenta and decidua. *Sci*
820 *Adv*. 2018. 4(10):eaau4788. Doi: 10.1126/sciadv.aau4788.
821 **23.** Liu Y, et al. Single-cell RNA-seq reveals the diversity of trophoblast subtypes and patterns of
822 differentiation in the human placenta. *Cell Res*. 2018. 28(8):8 19-832. Doi: 10.1038/s41422-018-
823 0066-y.
824 **24.** Meinhardt G, et al. Pivotal role of the transcriptional co-activator YAP in trophoblast stemness of
825 the developing human placenta. *Proc Natl Acad Sci USA*. 2020. 117(24): 13562-13570. Doi:
826 10.1073/pnas.2002630117.
827 **25.** Saha B, et al. TEAD4 ensures postimplantation development by promoting trophoblast self-
828 renewal: An implication in early human pregnancy loss. *Proc Natl Acad Sci USA*. 2020. 117(30):
829 17864-17875. Doi: 10.1073/pnas.2002449117.
830 **26.** Del Valle-Pérez B, et al. Wnt controls the transcriptional activity of Kaiso through CK1ε-dependent
831 phosphorylation of p120-catenin. *J Cell Sci*. 2016. 129(4): 873. Doi: 10.1242/jcs.186288.
832 **27.** Nemeth MJ, et al. Hmgb3 regulates the balance between hematopoietic stem cell self-renewal and
833 differentiation. *Proc Natl Acad Sci USA*. 2006. 103(37): 13783-8. Doi: 10.1073/pnas.0604006103.
834 **28.** Thomas G. An encore for ribosome biogenesis in the control of cell proliferation. *Nature*. 2000. 2:

835 E71-72.
836 **29.** Xu X, et al. The role of ribosomal proteins in the regulation of cell proliferation, tumorigenesis, and
837 genomic integrity. *Sci China Life*. 2016. 59(7): 656-672.
838 **30.** Khajuria RK, et al. Ribosome levels selectively regulate translation and lineage commitment in
839 human hematopoiesis. *Cell*. 2018. 173(1): Doi: 10.1016/j.cell.2018.02.036.
840 **31.** Shi Z, et al. DNA-binding mechanism of the Hippo pathway transcription factor TEAD4.
841 *Oncogene*. 2017. 36: 4362-4369. Doi: https://doi.org/10.1038/onc.2017.24.
842 **32.** Saha B, et al. TEAD4 ensures postimplantation development by promoting trophoblast self-
843 renewal: an implication in early human pregnancy loss. PNAS. 2020. 117(30): 17864-17875.
844 **33.** Xiao L, et al. Deciphering a distinct regulatory network of TEAD4, CDX2 and GATA3 in humans
845 for trophoblast transition from embryonic stem cells. *Biochim Biophys Acta Mol Cell Res*. 2020.
846 1867(9): 118736.
847 **34.** Yagi R, et al. Transcription factor TEAD4 specifies the trophectoderm lineage at the beginning of
848 mammalian development. *Development*. 2007. 134: 3827-3836. doi: 10.1242/dev.010223.
849 **35.** Ilicic T, et al. Classification of low quality cells from single-cell RNA-seq data. *Genome Biol*.
850 2016. 17(29). Doi: https://doi.org/10.1186/s13059-016-0888-1.
851 **36.** Galluzzi L, et al. Mitochondria: master regulators of danger signalling. *Nat Rev Mol Cell Biol*.
852 2012. 13: 780-788. Doi: https://doi.org/10.1038/nrm3479.
853 **37.** Detmer SA and Chan DC. Functions and dysfunctions of mitochondrial dynamics. *Nat Rev Mol*
854 *Cell Biol*. 2007. 8: 870-879. Doi: https://doi.org/10.1038/nrm2275.
855 **38.** Yoon JC, et al. Wnt signaling regulates mitochondrial physiology and insulin sensitivity. *Genes &*
856 *Dev*. 2010. 24: 1507-1518. Doi: 10.1101/gad.1924910.
857 **39.** Brown K, et al. WNT/β-catenin signaling regulates mitochondrial activity to alter the oncogenic
858 potential of melanoma in a PTEN-dependent manner. *Oncogene*. 2017. 36(22): 3119-3136. Doi:
859 10.1038/onc.2016.450.
860 **40.** Jauniaux E, et al. Onset of maternal arterial blood flow and placental oxidative stress. A possible
861 factor in human early pregnancy failure. *Am J Pathol*. 2000. 157(6): 2111-2122. Doi:
862 10.1016/S0002-9440(10)64849-3.
863 **41.** Jauniaux E, et al. Evaluation of respiratory gases and acid-base gradients in human fetal fluids and
864 uteroplacental tissue between 7 and 16 weeks' gestation. *Am J ObGyn*. 2001. 184(5): 998-1003.
865 **42.** Weiss G, et al. The trophoblast plug during early pregnancy: a deeper insight. *Histochem Cell Biol*.
866 2016. 146: 749-756. Doi: https://doi.org/10.1007/s00418-016-1474-z.

867 **43.** Tuuli MG, et al. Review: oxygen and trophoblast biology—a source of controversy. Placenta. 2011.
868 32(2): S109-S118. doi: 10.1016/j.placenta.2010.12.013.
869 **44.** Chang CW, et al. Trophoblast lineage specification, differentiation, and their regulation by oxygen
870 tension. J Endocrinol. 2018. 236(1): R43-56. Doi: https://doi.org/10.1530/JOE-17-0402.
871 **45.** Wakeland AK, et al. Hypoxia directs human extravillous trophoblast differentiation in a hypoxia-
872 inducible factor-dependent manner. Am J Pathol. 2017. 187(4): 767-780. Doi:
873 https://doi.org/10.1016/j.ajpath.2016.11.018.
874 **46.** Treissman J, et al. Low oxygen enhances trophoblast column growth by potentiating differentiation
875 of the extravillous lineage and promoting LOX activity. Development. 2020. 147(2). DOI:
876 10.1242/dev.181263.
877 **47.** Zen Q, et al. Critical factors in basal cell adhesion molecule/Lutheran-mediated adhesion to
878 laminin. J Biol Chem. 1999. 274(2): 728-734. Doi: https://doi.org/10.1074/jbc.274.2.728.
879 **48.** Kikkawa Y, et al. The Lutheran/basal cell adhesion molecule promotes tumor cell migration by
880 modulating integrin-mediated cell attachment to laminin-511 protein. J Biol Chem. 288(43): 30990-
881 31001. Doi: https://doi.org/10.1074/jbc.M113.486456.
882 **49.** Kannan K et al. Recurrent BCAM-AKT2 fusion gene leads to a constitutively activated AKT2
883 fusion kinase in high-grade serous ovarian carcinoma. PNAS. 2015. 112(11): E1272-1277. Doi:
884 10.1073/pnas.1501735112.
885 **50.** Jin J, et al. Upregulation of BCAM and its sense lncRNA BAN are associated with gastric cancer
886 metastasis and poor prognosis. Mol Oncology. 2020. 14(4): 829-845. Doi:
887 https://doi.org/10.1002/1878-0261.12638.
888 **51.** Akiyama H, et al. The FBI/Akirin2 target gene, BCAM, acts as a suppressive oncogene. PLOS
889 One. 2013. 8(11): e78716. Doi: https://doi.org/10.1371/journal.pone.0078716.
890 **52.** Collec E, et al. Novel role for the Lu/BCAM-spectrin interaction in actin cytoskeleton
891 reorganization. Biochem J. 2011. 436(3): 699-708. Doi: https://doi.org/10.1042/BJ20101717.
892 **53.** Liu M, et al. Laminins regulate placentation and pre-eclampsia: focus on trophoblasts and
893 endothelial cells. Front Cell Dev Biol. 2020. 8: 754-762. Doi:
894 https://doi.org/10.3389/fcell.2020.00754.
895 **54.** Butler A, et al. Integrating single-cell transcriptomic data across different conditions, technologies,
896 and species. *Nature Biotechnol*. 2018. 36(5): 411-420.
897 **55.** Stuart T, et al. Comprehensive integration of single-cell data. *Cell*. 2019. 177(7): 1888-1902.
898 **56.** McGinnis CS, et al. DoubletFinder: Doublet detection in single-cell RNA sequencing data using

899 artificial nearest neighbours. Cell Systems. 2019. 8(4): 329-337.
900 **57.** Finak G, et al. MAST: a flexible statistical framework for assessing transcriptional changes and
901 characterizing heterogeneity in single-cell RNA sequencing data. *Genome Biol*. 2015. 16: 278.
902 **58.** Yu G, et al. clusterProfiler: an R package for comparing biological themes among gene clusters.
903 *OMICS*. 2012. 16(5): 284-287.
904 **59.** Janky R, et al. iRegulon: from a gene list to a gene regulatory network using large motif and track
905 collections. *PLoS Comput Biol*. 2014. 10(7): e1003731.
906 **60.** Trapnell C, Cacchiarella D, et al. The dynamics and regulators of cell fate decisions are revealed by
907 pseudo-temporal ordering of single cells. *Nature Biotechnol*. 2014. 32(4): 381.
908 **61.** Qiu X, Hill A, Trapnell C, et al. Single-cell mRNA quantification and differential analysis with
909 Census. *Nat Methods*. 2017. 14(3): 309-315.
910 **62.** Qiu X, Trapnell C, et al. Reverse graph embedding resolves complex single-cell developmental
911 trajectories. *Nat Methods*. 2017. 14(10): 979-982.
912 **63.** Cao J, et al. The single-cell transcriptional landscape of mammalian organogenesis. *Nature*. 2019.
913 566(7745): 496-502. Doi: 10.1038/s41586-019-0969-x.
914 **64.** La Manno G, et al. RNA velocity of single cells. *Nature*. 2018. 560: 494-498.
915 **65.** Bergen V, et al. Generalizing RNA velocity to transient cell states through dynamical modelling.
916 Nature Biotechnol. 2020: https://doi.org/10.1038/s41587-020-0591-3
917 **66.** Teschendorff A, Enver T. Single-cell entropy for accurate estimation of differentiation potency
918 from a cell's transcriptome. *Nat Commun*. 2017. 8(1): 1-15.

919

920 **TITLES AND LEGENDS TO FIGURES**

921 **Figure 1: Single cell characterization of first trimester trophoblasts**
922
923 **(A)** Schematic of a first trimester chorionic villous including anatomical representations of both an
924 anchoring villous and floating villous. Highlighted are trophoblast sub-populations and the villous and
925 extravillous cell differentiation trajectories: cytotrophoblast (CTB), column cytotrophoblast (cCTB),
926 syncytiotrophoblast (SCT), and invasive extravillous trophoblast (EVT).
927 **(B)** Summary of workflow used for collection, processing, and single cell analysis of placental villous
928 cells. MFI, Maternal-Fetal Interface, 7AAD: 7-Aminoactinomycin D, FSC-A: Forward Scatter Area.
929 **(C)** Uniform Manifold Approximation and Projection (UMAP) plot of 7798 captured trophoblasts,
930 demonstrating 8 distinct trophoblast clusters: CTB1-4, cCTB1-2, SCTp, and EVT.
931 **(D)** Heatmap showing the average expression of known trophoblast and proliferation gene markers in
932 each trophoblast cluster. Cell cluster names and colours correspond to those in Figure 1C.
933 **(E)** Stacked bar plot showing cell state distribution in distinct phases of the cell cycle (G1, G2M, S).
934 **(F)** UMAP plots showing expression (red) of CTB progenitor (*EGFR*, *TP63*), proliferation (*MKI67*),
935 EVT (*HLA-G*), SCT (*ERVFRD-1*), and an EVT progenitor (*ITGA2*) gene(s).
936 **(G)** Proportion of 4687 early first trimester trophoblasts in each scRNA-seq-defined state in early (6-7
937 weeks) and late (9-12 weeks) gestational time-points.

Figure 1

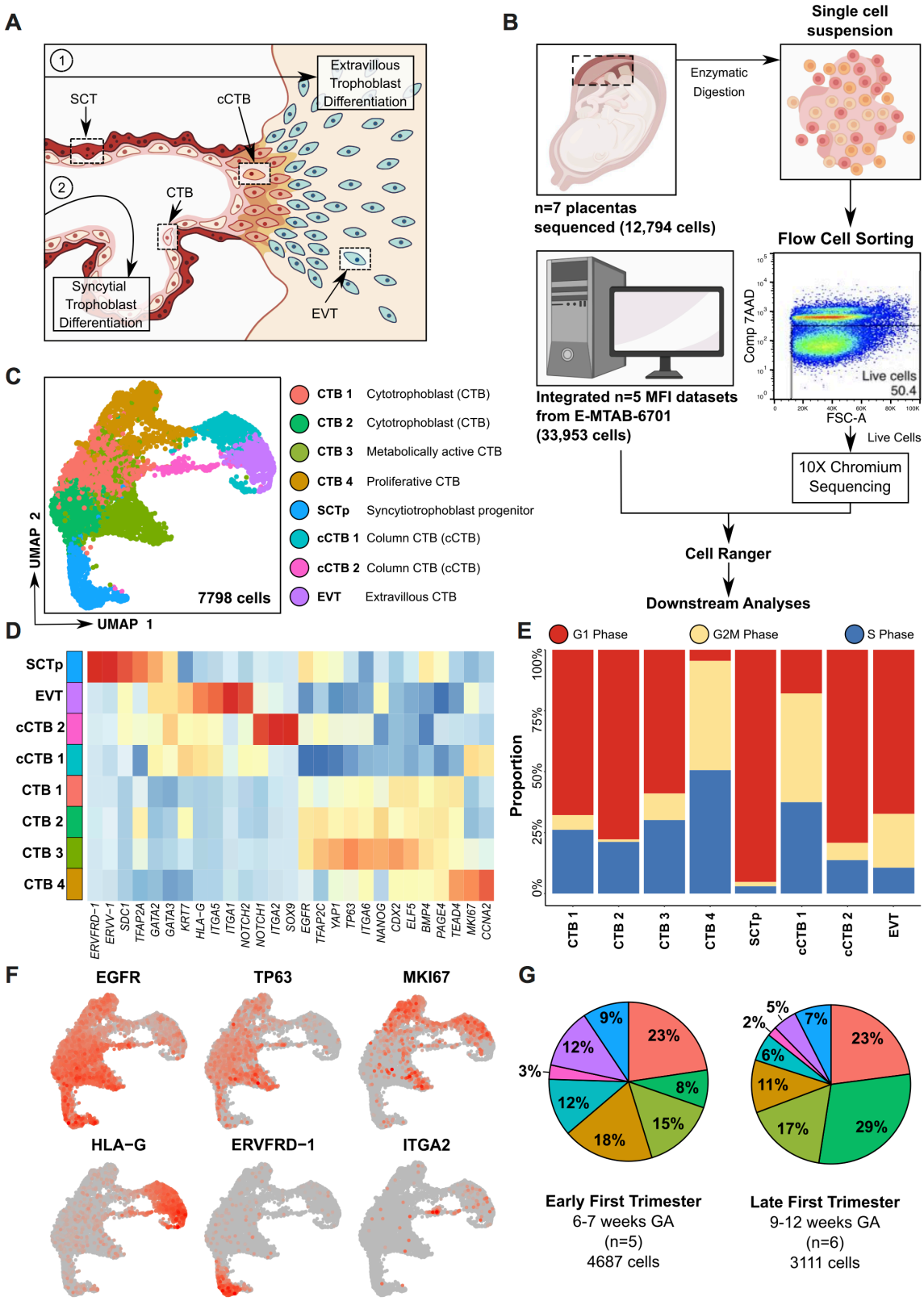
A
1
Extravillous Trophoblast Differentiation
SCT
cCTB
2
CTB
Syncytial Trophoblast Differentiation
EVT
B
Single cell suspension
Enzymatic Digestion
n=7 placentas sequenced (12,794 cells)
Flow Cell Sorting
Comp 7AAD
Live cells 50.4
FSC-A
Live Cells
Integrated n=5 MFI datasets from E-MTAB-6701 (33,953 cells)
10X Chromium Sequencing
Cell Ranger
Downstream Analyses
C
UMAP 2
UMAP 1
7798 cells
CTB 1 Cytotrophoblast (CTB)
CTB 2 Cytotrophoblast (CTB)
CTB 3 Metabolically active CTB
CTB 4 Proliferative CTB
SCTp Syncytiotrophoblast progenitor
cCTB 1 Column CTB (cCTB)
cCTB 2 Column CTB (cCTB)
EVT Extravillous CTB
D
SCTp
EVT
cCTB 2
cCTB 1
CTB 1
CTB 2
CTB 3
CTB 4
ERVFRD−1 ERVV−1 SDC1 TFAP2A GATA2 GATA3 KRT7 HLA−G ITGA5 ITGA1 NOTCH2 NOTCH1 ITGA2 SOX9 EGFR TFAP2C YAP1 TP63 ITGA6 NANOG CDX2 ELF5 BMP4 PAGE4 TEAD4 MKI67 CCNA2
E
G1 Phase
G2M Phase
S Phase
Proportion
0% 25% 50% 75% 100%
CTB 1 CTB 2 CTB 3 CTB 4 SCTp cCTB 1 cCTB 2 EVT
F
EGFR
TP63
MKI67
HLA−G
ERVFRD−1
ITGA2
G
23% 8% 15% 18% 12% 3% 12% 9%
Early First Trimester
6-7 weeks GA
(n=5)
4687 cells
23% 29% 17% 11% 6% 2% 5% 7%
Late First Trimester
9-12 weeks GA
(n=6)
3111 cells

938 **Figure 2: Single cell transcriptomic resolution of distinct CTB states**
939
940 **(A)** UMAP plot of 5477 captured CTBs highlighting 4 distinct states.
941 **(B)** Heatmap showing the average expression of the top-10 genes specific to each CTB state.
942 **(C)** Venn diagram comparing the intersection of genes upregulated within each CTB1-4 states.
943 **(D)** Dot plots of the top significant terms enriched by gene ontology analysis informed by gene
944 signatures enriched within distinct CTB (CTB1-4) states.
945 **(I)** Heatmap showing the average expression of transcription factors identified as putative
946 regulators/drivers enriched within CTB1-4 states.
947

Figure 2

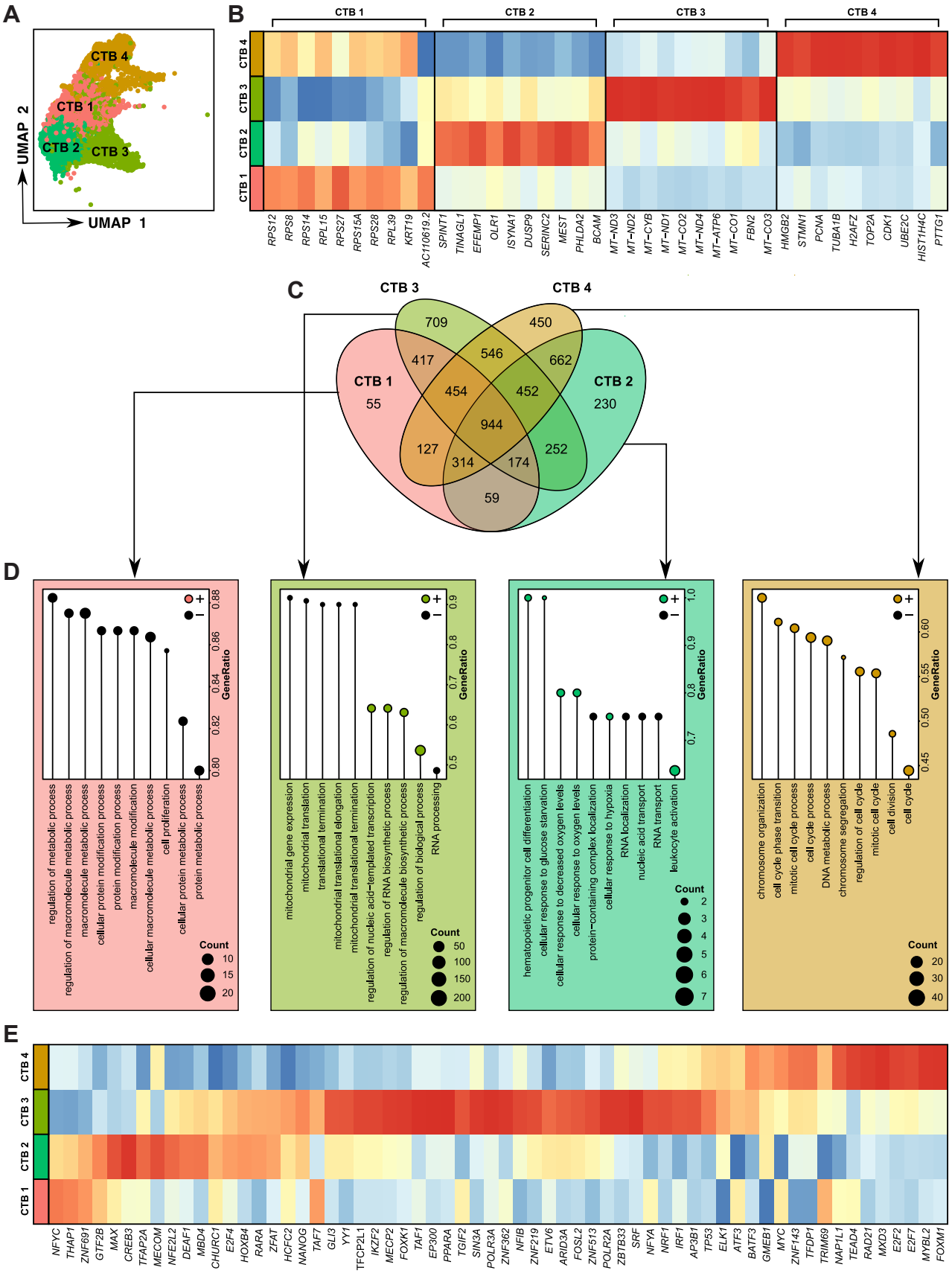
A
CTB 4
CTB 1
CTB 2
CTB 3
UMAP 2
UMAP 1
B
CTB 1
CTB 2
CTB 3
CTB 4
RPS12 RPS8 RPS14 RPL15 RPS27 RPS15A RPS28 RPL39 KRT19 AC110619.2
SPINT1 TINAGL1 EFEMP1 OLR1 ISYNA1 DUSP9 SERINC2 MEST PHLDA2 BCAM
MT-ND3 MT-ND2 MT-CYB MT-ND1 MT-CO2 MT-ND4 MT-ATP6 MT-CO1 FBN2 MT-CO3
HMGB2 STMN1 PCNA TUBA1B H2AFZ TOP2A CDK1 UBE2C HIST1H4C PTTG1
C
CTB 3
CTB 4
CTB 1
55
CTB 2
230
709
450
417
546
662
454
452
944
127
252
314
174
59
D
regulation of metabolic process
regulation of macromolecule metabolic process
macromolecule metabolic process
cellular protein modification process
protein modification process
macromolecule modification
cellular macromolecule metabolic process
cell proliferation
cellular protein metabolic process
protein metabolic process
GeneRatio
Count
mitochondrial gene expression
mitochondrial translation
translational termination
mitochondrial translational elongation
mitochondrial translational termination
regulation of nucleic acid-templated transcription
regulation of RNA biosynthetic process
regulation of macromolecule biosynthetic process
regulation of biological process
RNA processing
hematopoietic progenitor cell differentiation
cellular response to glucose starvation
cellular response to decreased oxygen levels
cellular response to oxygen levels
protein-containing complex localization
cellular response to hypoxia
RNA localization
nucleic acid transport
RNA transport
leukocyte activation
chromosome organization
cell cycle phase transition
mitotic cell cycle process
cell cycle process
DNA metabolic process
chromosome segregation
regulation of cell cycle
mitotic cell cycle
cell division
cell cycle
E
CTB 1
CTB 2
CTB 3
CTB 4
NFYC THAP1 ZNF691 GTF2B MAX CREB3 TFAP2A MECOM NFE2L2 DEAF1 MBD4 CHURC1 E2F4 HOXB4 RARA ZFAT HCFC2 NANOG TAF7 GLI3 YY1 TFCP2L1 IKZF2 MECP2 FOXK1 TAF1 EP300 PPARA TGIF2 SIN3A POLR3A ZNF362 NFIB ZNF219 ETV6 ARID3A FOSL2 ZNF513 POLR2A ZBTB33 SRF NFYA NRF1 IRF1 AP3B1 TP53 ELK1 ATF3 BATF3 GMEB1 MYC ZNF143 TFDP1 TRIM69 NAP1L1 TEAD4 RAD21 MXD3 E2F2 E2F7 MYBL2 FOXM1

Figure 3: scVelo-informed cell differentiation identifies a primitive CTB origin.

(A) UMAP plot overlain with projected RNA velocity (scVelo) vector field, indicating trophoblast directionality (represented by the velocity arrows) away from a putative origin towards endpoint SCTp and EVT states. Cell cluster names and colours correspond to those in Figure 1C.
(B) UMAP plots showing gene expression (red) of progenitor- and stem cell-associated genes in all scRNA-seq-informed trophoblast states.
(C) Venn diagram comparing the genes upregulated within CTB states 2 and 3. Highlighted are genes related to WNT and EGFR signaling pathways, genes involved in extracellular matrix (ECM) interactions, and miscellaneous (Misc) genes of interest.
(D) Scatter plots showing gene expression levels of EGFR related genes (*EFEMP1*), transcription factors (*EGR1* and *ELF5*), and genes involved in ECM-cell interactions (*ITGA6*, *BCAM*, and *LAMA5*) across pseudotime as the CTB2 state transitions to the CTB3 state.
(E) UMAP plots showing gene expression (red) of genes upregulated within the CTB2 state origin.

Figure 3

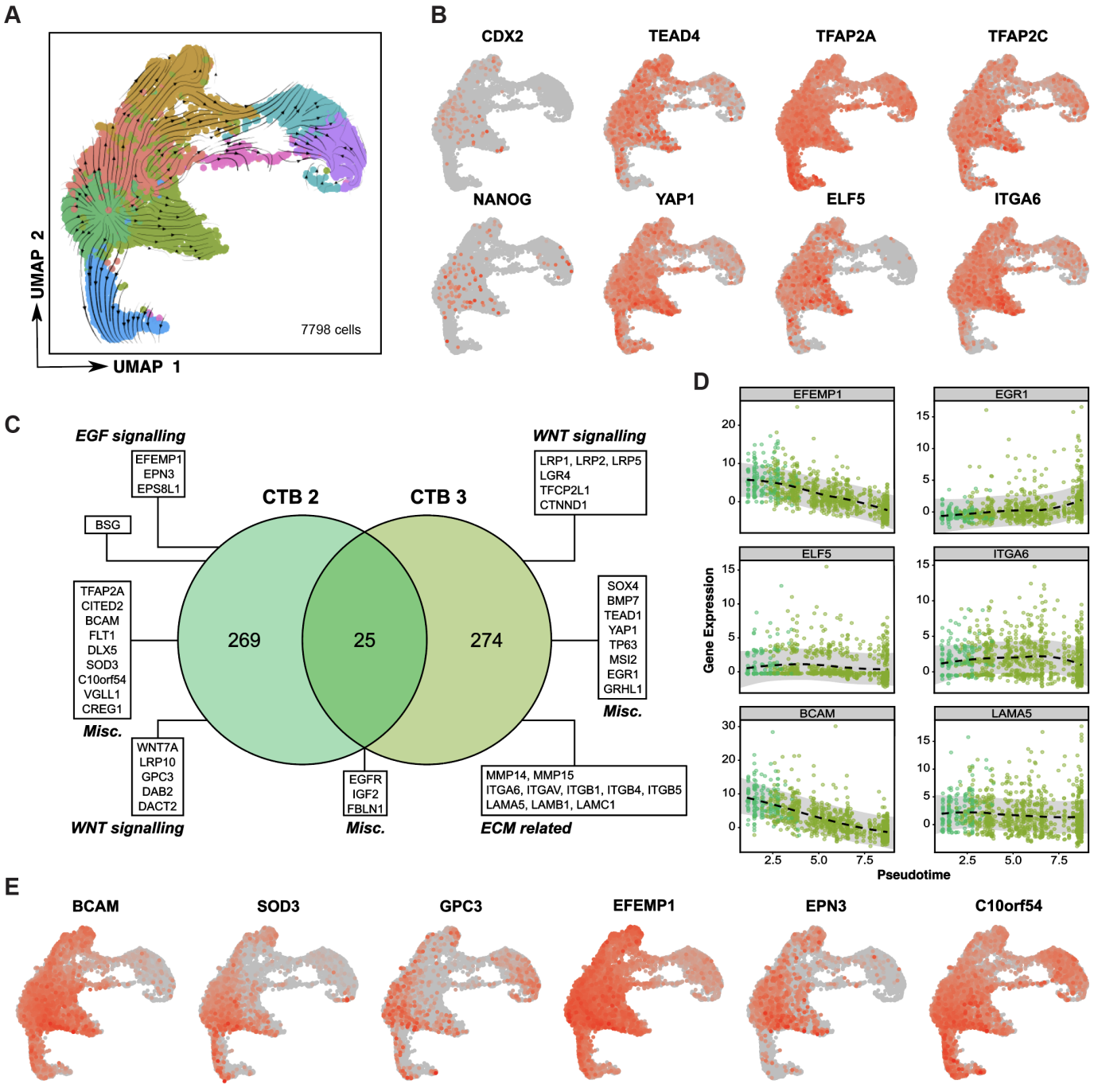
A
UMAP 2
UMAP 1
7798 cells
B
CDX2
TEAD4
TFAP2A
TFAP2C
NANOG
YAP1
ELF5
ITGA6
C
EGF signalling
EFEMP1
EPN3
EPS8L1
BSG
WNT signalling
LRP1, LRP2, LRP5
LGR4
TFCP2L1
CTNND1
CTB 2
CTB 3
269
25
274
TFAP2A
CITED2
BCAM
FLT1
DLX5
SOD3
C10orf54
VGLL1
CREG1
Misc.
SOX4
BMP7
TEAD1
YAP1
TP63
MSI2
EGR1
GRHL1
Misc.
WNT7A
LRP10
GPC3
DAB2
DACT2
WNT signalling
EGFR
IGF2
FBLN1
Misc.
MMP14, MMP15
ITGA6, ITGAV, ITGB1, ITGB4, ITGB5
LAMA5, LAMB1, LAMC1
ECM related
D
EFEMP1
EGR1
ELF5
ITGA6
BCAM
LAMA5
Gene Expression
Pseudotime
E
BCAM
SOD3
GPC3
EFEMP1
EPN3
C10orf54

963 **Figure 4: Single cell transcriptomic analyses in hTSC organoids recapitulate a primitive CTB**
964 **origin**
965
966 **(A)** Bright field microscopy images of regenerative (Wnt+) and EVT-differentiated (Wnt-) hTSC-
967 derived organoids following 10 days of culture. Bar = 400 μm.
968 **(B)** Flow cytometry plots showing cell frequencies of HLA-G, CD49e, and HLA-ABC positive cells in
969 regenerative (Wnt+) and EVT-differentiated hTSC-derived (CT27) organoids.
970 **(C)** Relative measurement of mRNA levels by qPCR in EVT-differentiated hTSC-derived organoids
971 (CT27, CT29, CT30) over 21 days (D) of culture. Shown are CTB/progenitor (TEAD4, ITGA6),
972 syncytial (CGB, CSH1), immature EVT (ITGA5, NOTCH1), and mature EVT (NOTCH2, HLA-G)
973 genes.
974 **(D)** UMAP and gene heatmap plots of combined CT27, CT29, and CT30 single cell hTSCs following
975 culture in regenerative (Wnt+) and EVT-differentiated (Wnt-) conditions after 7 days in culture.
976 UMAP plots are overlain with projected RNA velocity (scVelo) vector field, demonstrating 7 distinct
977 trophoblast clusters representing 3 states (CTB1, CTB2, CTB3, bipotent cCTB, EVT1, EVT2, SCTp).
978 Heatmap shows the average expression of trophoblast- and proliferation-associated genes in each cell
979 state.
980 **(E)** UMAP and gene heatmap plots derived from individual hTSC lines (CT27, 2259 cells; CT29, 1446
981 cells; CT30, 2604 cells) subjected to scRNA-seq analyses. UMAP plots are overlain with projected
982 RNA velocity vector field, demonstrating 5 distinct trophoblast clusters in each hTSC line.
983 **(F)** Venn diagram comparing genes shared and distinct between CTB2/CTB3 in chorionic villi and
984 CTB1/CTB2 states in hTSC organoids.
985 UMAP plots showing expression of BCAM (red) in **(G)** combined (CT27, CT29, CT30) and **(H)**
986 segregated hTSC-derived organoid cells/states.
987

Figure 4

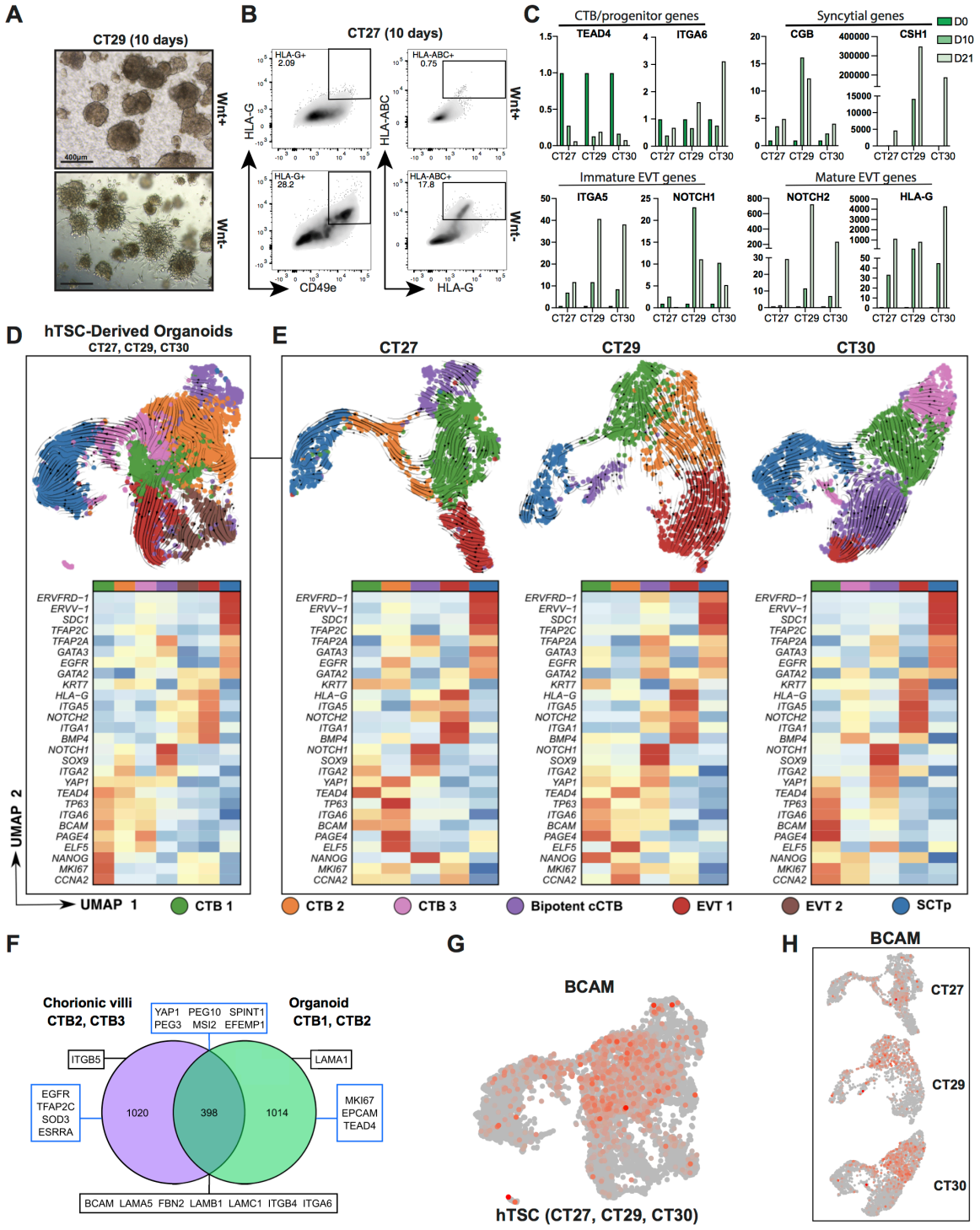
A
CT29 (10 days)
Wnt+
Wnt-
400µm
B
CT27 (10 days)
HLA-G+
2.09
HLA-ABC+
0.75
HLA-G+
28.2
HLA-ABC+
17.8
HLA-G
HLA-ABC
CD49e
HLA-G
C
CTB/progenitor genes
TEAD4
ITGA6
Syncytial genes
CGB
CSH1
D0
D10
D21
Immature EVT genes
ITGA5
NOTCH1
Mature EVT genes
NOTCH2
HLA-G
CT27 CT29 CT30
D
hTSC-Derived Organoids
CT27, CT29, CT30
UMAP 2
UMAP 1
E
CT27
CT29
CT30
ERVFRD-1
ERVV-1
SDC1
TFAP2C
TFAP2A
GATA3
EGFR
GATA2
KRT7
HLA-G
ITGA5
NOTCH2
ITGA1
BMP4
NOTCH1
SOX9
ITGA2
YAP1
TEAD4
TP63
ITGA6
BCAM
PAGE4
ELF5
NANOG
MKI67
CCNA2
CTB 1
CTB 2
CTB 3
Bipotent cCTB
EVT 1
EVT 2
SCTp
F
Chorionic villi
CTB2, CTB3
Organoid
CTB1, CTB2
YAP1 PEG10 SPINT1
PEG3 MSI2 EFEMP1
ITGB5
LAMA1
EGFR
TFAP2C
SOD3
ESRRA
1020
398
1014
MKI67
EPCAM
TEAD4
BCAM LAMA5 FBN2 LAMB1 LAMC1 ITGB4 ITGA6
G
BCAM
hTSC (CT27, CT29, CT30)
H
BCAM
CT27
CT29
CT30

988 **Figure 5: BCAM enrichment establishes a regenerative/growth advantage in trophoblast**
989 **organoids**
990
991 **(A)** Immunofluorescence (IF) images of BCAM and keratin-7 (KRT7), human chorionic gonadotrophin
992 (hCG), and HLA-G in early (6.3 weeks) and late (11.2 weeks) first trimester placental villi. Nuclei are
993 stained with DAPI (white). Bars = 100μm.
994 **(B)** IF images of BCAM, hCG and Ki67 in hTSC-derived organoid (CT29) cultured in regenerative
995 (Wnt+) media for 7 days.
996 **(C)** Cell sorting workflow for isolating $BCAM^{hi}$ and $BCAM^{lo}$ EGFR+ CTBs in hTSC (CT29)-derived
997 organoids.
998 **(D)** Bright field images of hTSC (CT29) $BCAM^{hi}$ and $BCAM^{lo}$ –derived organoids cultured over 11
999 days in regenerative Wnt+ media. Bars = 200μm.
1000 **(E)** Colony area (μm^2) of $BCAM^{hi}$ and $BCAM^{lo}$ hTSC (CT29)-derived organoids cultured over 11 days
1001 (D).
1002 **(F)** Flow cytometric panels showing expression of BCAM and EGFR in $BCAM^{hi}$ and $BCAM^{lo}$, CT29-
1003 derived organoids following 11 days of culture.
1004 **(G)** Heatmap showing levels of select differentially expressed genes from CTB expressing high (hi) or
1005 low (lo) levels of *BCAM* in the CTB1 state of CT29-derived organoids following 7 days of culture.

Figure 5

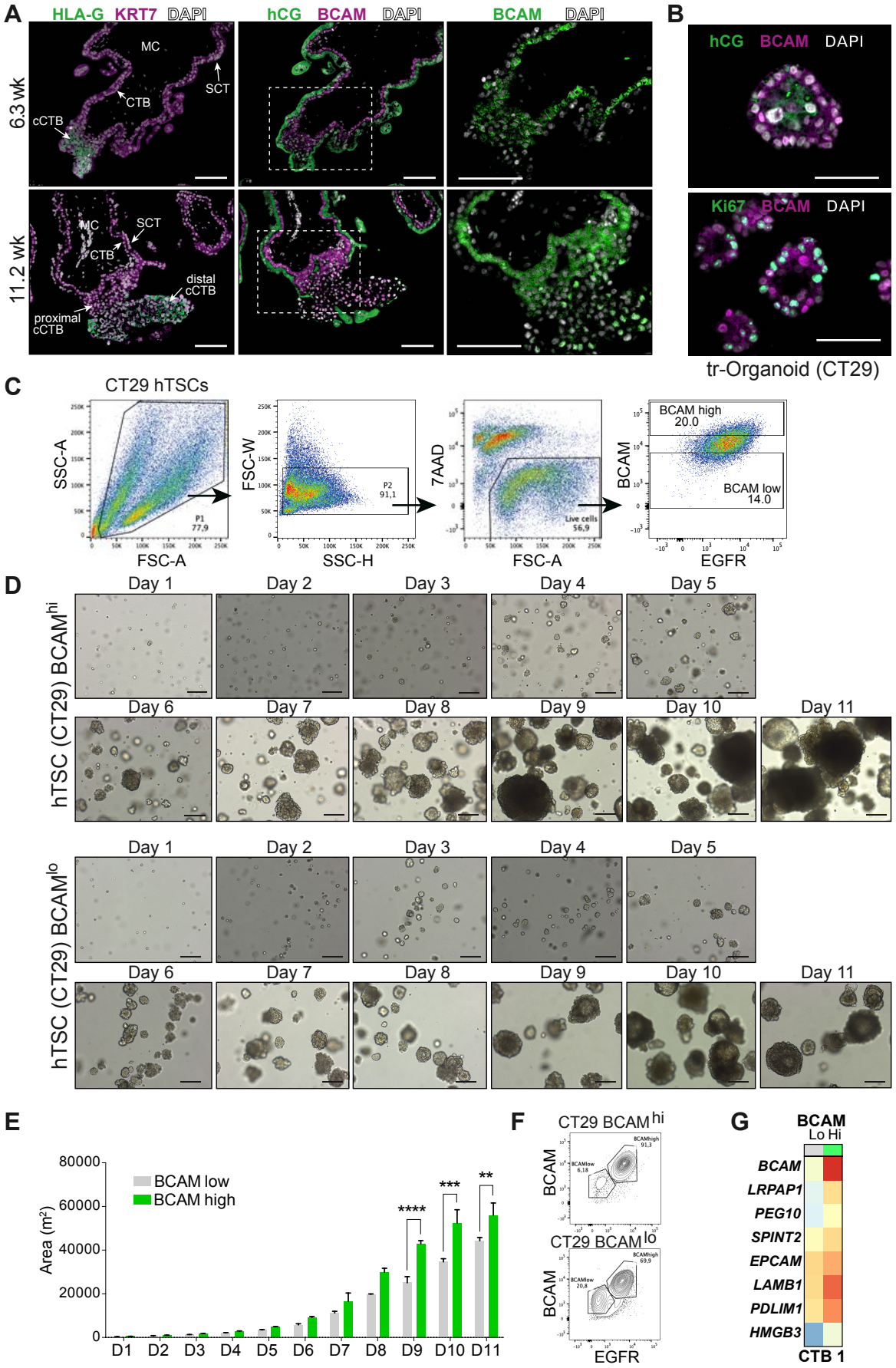
A
HLA-G KRT7 DAPI
hCG BCAM DAPI
BCAM DAPI
6.3 wk
11.2 wk
MC
SCT
CTB
cCTB
distal cCTB
proximal cCTB
B
hCG BCAM DAPI
Ki67 BCAM DAPI
tr-Organoid (CT29)
C
CT29 hTSCs
SSC-A
FSC-A
P1 77,9
FSC-W
SSC-H
P2 91,1
7AAD
FSC-A
Live cells 56,9
BCAM
EGFR
BCAM high 20.0
BCAM low 14.0
D
hTSC (CT29) BCAM hi
hTSC (CT29) BCAM lo
Day 1
Day 2
Day 3
Day 4
Day 5
Day 6
Day 7
Day 8
Day 9
Day 10
Day 11
E
Area (m²)
BCAM low
BCAM high
D1 D2 D3 D4 D5 D6 D7 D8 D9 D10 D11
****
***
**
F
CT29 BCAM hi
CT29 BCAM lo
BCAM
EGFR
G
BCAM
Lo Hi
BCAM
LRPAP1
PEG10
SPINT2
EPCAM
LAMB1
PDLIM1
HMGB3
CTB 1

1006 **Supplemental Figure 1: Sample quality control and single cell characterization of the first**
1007 **trimester human maternal-fetal interface**
1008
1009 **(A – C)** Violin plots showing the distribution of the raw number of features **(A)**, the raw number of
1010 counts **(B)**, and the percent mitochondrial DNA content remaining post quality control and data pre-
1011 processing **(C)** captured per cell during sequencing for each sample. Samples 1-6 (teal) represent the
1012 placental tissue samples sequenced by the Beristain lab, samples 7-11 (red) represent the placental
1013 tissue samples acquired from ArrayExpress, and samples 12-15 (grey) represent the decidual tissue
1014 samples acquired from ArrayExpress.
1015 **(D)** Scatter plot showing the distribution of captured cells across principal components 1 and 2
1016 following dimensional reduction in principal component space. Cell positions are calculated based on
1017 cell embeddings calculated during dimensional reduction by principal component analysis. Cells are
1018 colour coordinated by source with teal representing those cells originating from placental tissue
1019 samples sequenced by the Beristain lab and red representing those cells originating from placental and
1020 decidual tissue samples acquired from ArrayExpress.
1021 **(E)** UMAP plot of 50,790 captured cells, demonstrating 31 distinct clusters identified within the first
1022 trimester human maternal fetal interface. Dashed lines separate maternal decidual immune cells from
1023 non-immune cells and fetal placental trophoblasts. Cells are colour coordinated by identity and
1024 abbreviations are identical to those in Figure 1A. Epigland: epiglandular cell, fetal Endo: fetal
1025 endothelial cell, dEndo: decidual endothelial cell, dSC: decidual stromal cell PV: perivascular cell,
1026 pFib: placental fibroblast, Hb: fetal Hofbauer cell, M1: macrophage cell 1, M2: macrophage cell 2,
1027 uNK: uterine natural killer cell.
1028 **(F)** UMAP projection of the captured maternal fetal interface cells, stratified by gestational age. Early
1029 (left panel): 9803 early first trimester cells from each identified cluster captured between 6-7 weeks
1030 gestational age, before the onset of maternal placental vascularization. Late (right panel): 40,987 late
1031 first trimester cells from each identified cluster captured between 9-12 weeks gestational age, after the
1032 onset of maternal placental vascularization. Cell cluster names and colours correspond to those in
1033 Supplemental Figure 1E.
1034 **(G)** Heatmap showing the average expression of known immune, non-immune, and trophoblast gene
1035 markers, as well as proliferation gene markers in each identified cluster. Cell cluster names and colours
1036 correspond to those in Supplemental Figure 1E.
1037 **(H)** Stacked bar plot showing the percent distribution of cells in each cluster with gene signatures
1038 representing a cell in the gap 1 phase of proliferation, the gap 2 or mitotic phases of proliferation, or the
1039 synthesis phase of proliferation. Cell cluster names and colours correspond to those in Supplemental
1040 Figure 1E and abbreviations are identical to those in Figure 1F.
1041 **(I)** UMAP plots showing gene expression in red of a mesenchymal cell gene marker (*VIM*), an immune
1042 cell gene marker (*PTPRC*, encoding the CD45 protein), endothelial cell gene markers (*CD34* and
1043 *VCAM1*), and a fibroblast gene marker (*ACTA2*).
1044 **(J)** UMAP plots showing gene expression in red of known trophoblast gene markers used to subset and
1045 purify first trimester human trophoblasts from other cells within the maternal fetal interface.
1046

1047

1048 **Supplemental Figure 2: Branched pseudotime ordering reveals increased complexity in the**
1049 **differentiation of CTB progenitors into mature SCT and EVT**
1050
1051 **(A)** Pseudotime trajectory plot showing trophoblasts ordered along the branched trajectory. Cells are
1052 colour coordinated by pseudotime value, with pseudotime increasing as cells move away from the root
1053 along the trajectory.
1054 **(B)** Cells are colour coordinated by cluster identity, with progress towards SCT indicated with a dashed
1055 arrow and progress towards EVT indicated with a solid arrow, moving away from the indicated
1056 trajectory root. Cell cluster names and colours correspond to those in Figure 1C.
1057
1058 Branched pseudotime heatmap showing relative gene expression changes and average cluster gene
1059 expression levels, respectively, of genes involved in **(A and B)** the WNT signaling pathway, **(C and D)**
1060 the HIPPO signaling pathway, **(E and F)** the NOTCH signaling pathway, and **(G and H)** the EGFR
1061 signaling pathway, all previously demonstrated to be involved in trophoblast maintenance and
1062 differentiation, as progenitor CTBs differentiate into either SCT or EVT.
1063
1064
1065 **Supplemental Figure 3: Additional pseudotime and Shannon entropy quantification supports**
1066 **identification of a cytotrophoblast stem cell niche**
1067
1068 **(A)** UMAP plot with constructed trajectory graph overlain. Cells are colour coordinated by relative
1069 pseudotime value.
1070 **(B)** UMAP plot with constructed trajectory graph overlain. Cells are colour coordinated by cluster
1071 identity. Cell cluster names and colours correspond to those in Figure 1C.
1072 **(C)** UMAP plot highlighting the constructed trajectory graph which describes the path taken as CTB
1073 state 2 progresses into CTB state 3. Cells are colour coordinated by cluster. Cluster names and colours
1074 correspond to those in Figure 1C.
1075
1076 **Supplemental Figure 4: Organoid colonies in BCAM^{hi} and BCAM^{lo} sorted organoids**
1077 Bar graph shows the average of numbers of organoid colonies from BCAM^{hi} and BCAM^{lo} –sorted
1078 CT29 organoids cultured over 11 days. Grey bars = BCAM^{lo}; Green bars = BCAM^{hi}.

Supplemental Figure 1

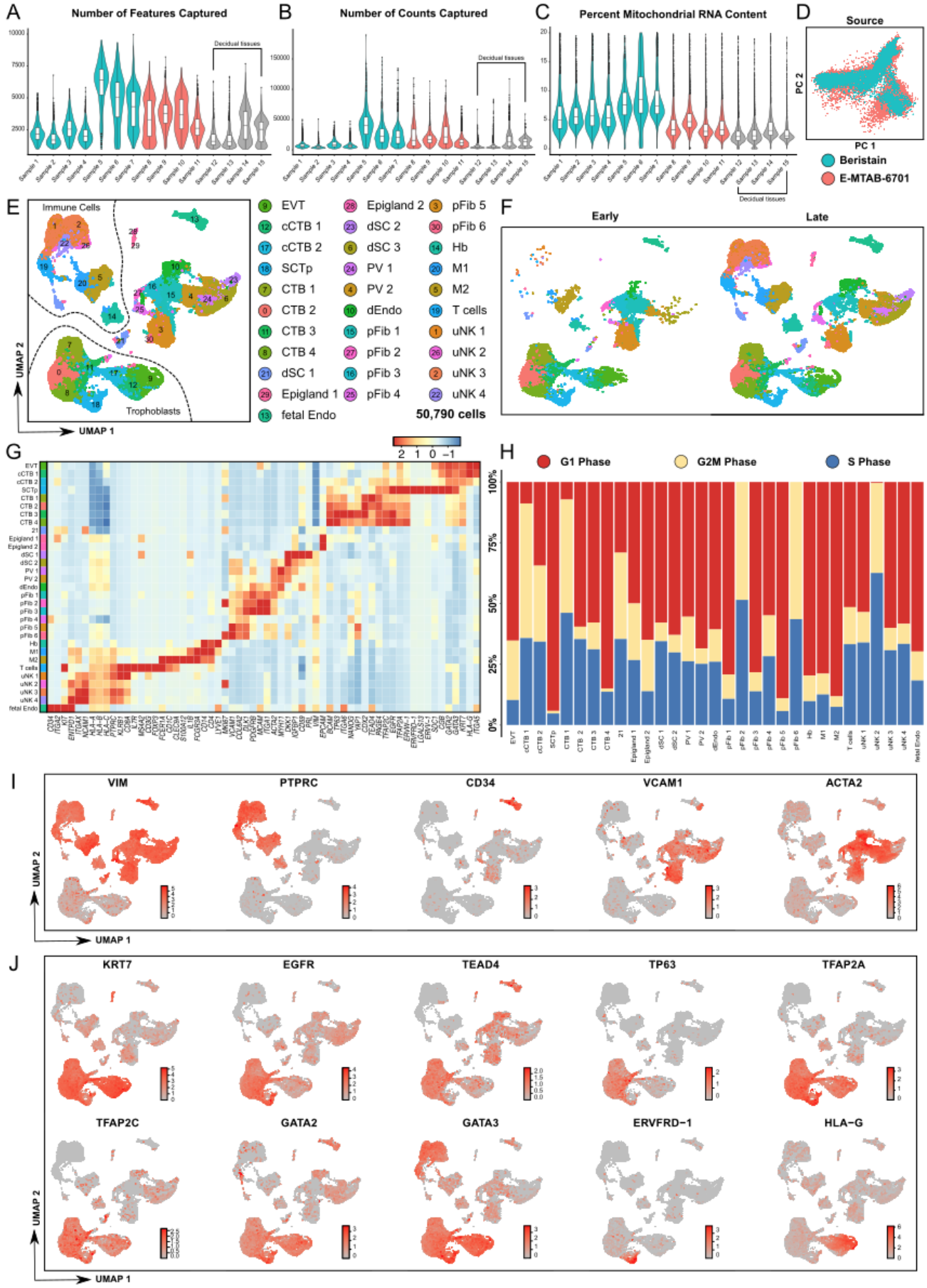

Supplemental Figure 2

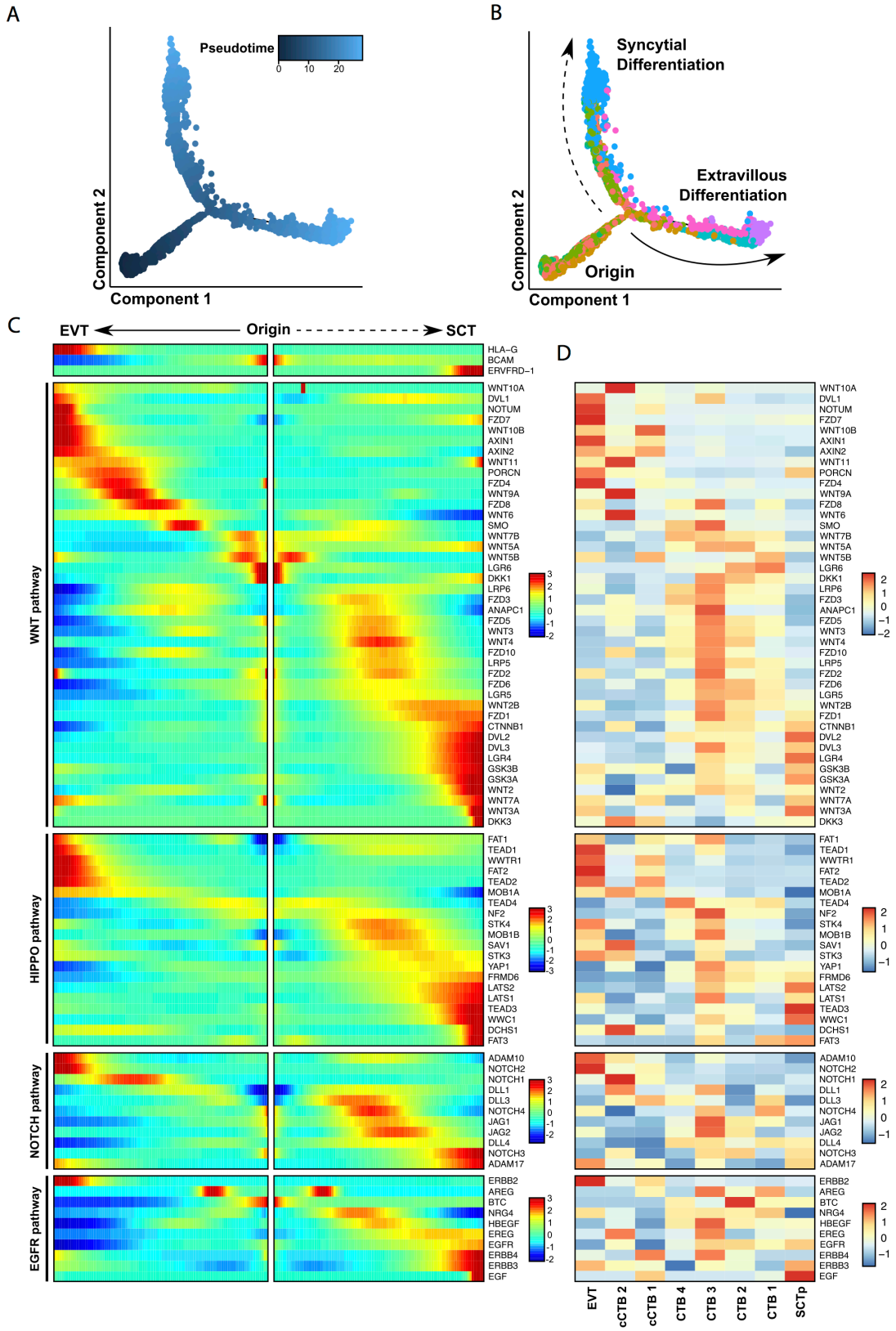

Supplemental Figure 3

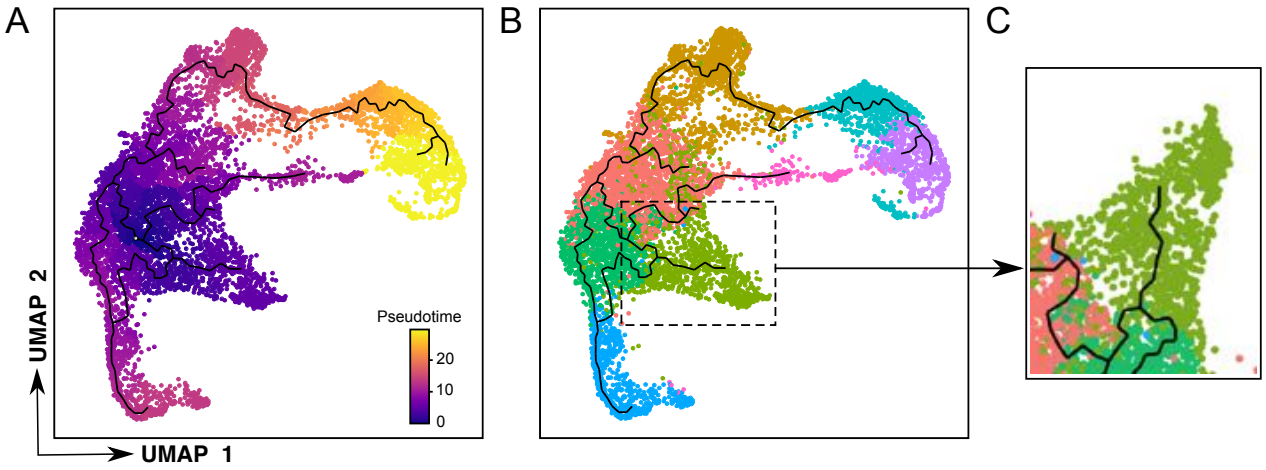
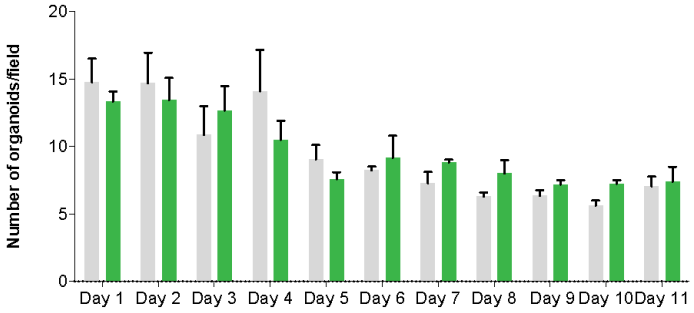
Supplemental Figure 4